SIMULATING THE EFFECTS OF DAM BREAKAGE ON THE DOWNSTREAM TOPOGRAPHY: MORPHOLOGICAL EVOLUTION OF MOUNDS AND A FURROW

Magua Amos Ng'ang'a (M.Sc.)
Reg. No. I84/25459/2011

A thesis submitted in partial fullfilment for the Degree of Doctor of Philosophy (Ph.D) in Applied Mathematics in the School of Pure and Applied Sciences of Kenyatta University

DECEMBER 2015

Declaration

This thesis is my original work and has not been presented for a degree award in any other university or for any other award.

Amos Ng'ang'a Magua
Signature..... Date.....

This thesis has been submitted for examination with our approval as university supervisors.

Dr. David Malonza
Signature..... Date.....
Department of Mathematics
Kenyatta University

Dr. Mark Kimathi
Signature..... Date.....
Department of Mathematics
Technical University of Kenya

Dr. Isaac Chepkwony
Signature..... Date.....
Department of Mathematics
Kenyatta University

Dedication

To my dear parents the late Welsh Magua and the late Loise Mary Ng'endo.

Acknowledgements

My sincere thanks, glory and honour goes to the Almighty God for his unfailing provision, protection and sustenance throughout the study period.

I am greatly indebted to my supervisors, Dr. Mark Kimathi who has tirelessly inspired me to undertake this dissertation. His timely encouragement, friendship and support have not only made the completion of this dissertation possible but has left an impression which will continue to influence my work. Dr. David Malonza and Dr. Isaac Chepkwony who apart from being my lecturers and giving me good background in modelling made enthusiastic participation, valuable suggestions and continuous encouragement during the dissertation.

I specially thank Prof. Francis Gatheri for reading my work and giving valuable suggestions.

Acknowledgment is also extended to Dr. Benard Kivunge the Chairman Mathematics department for his warm friendship and his continuous encouragement during the dissertation.

I extend my gratitude to Dr. Kube Ananda and Mr. Fidelis Magero for their invaluable assistance in inducting me to the latex typesetting system.

I sincerely thank the Dean's office for the financial support i received through the dean's research grant which boosted and enhanced the undertaking of this dissertation. Special thanks also to AMMSI for the sponsorship to the First Kenyatta University Mathematics Conference.

I extend special thanks to my wife Mukami, my daughters Ng'endo and Murugi and my son Magua for their love, understanding and prayers and for patiently enduring the many sacrifices as a result of this dissertation.

Table of Contents

List of Figures

Nomenclature

B	Height of the river bed
Bu	The volumetric load transport in the x direction
Bv	The volumetric load transport in the y direction
B_x	The bed topographic elevation in the x direction
B_y	The bed topographic elevation in the y direction
hu	Fluid flow rate in the x direction
hv	Fluid flow rate in the y direction
U	Vector of conserved variables of the morphodynamic modelling
F	Vector of convective flux in x direction of the morphodynamic component
Fr	Froude number
$S(U)$	source term of the morphodynamic component
G	Vector of convective flux in y direction of the morphodynamic component
g	Acceleration due to gravity
h	Water height
i	Index
I	Identity matrix
L	Wave length
P	Pressure
q_1	The volumetric sediment transport rate in the x direction
q_2	The volumetric sediment transport rate in the y direction
n	The time level
S	Source term vector
S_{fx}	Friction in the x direction
S_{fy}	Friction in the y direction
$\tilde{S}$	Source term in the y direction
$\tilde{\tilde{S}}$	Source term in the x direction
t	time
$\vec{V}$	Velocity of the fluid
$\vec{u}$	Velocity component in the x direction
$\vec{v}$	Velocity component in the y direction
$\vec{w}$	Velocity component in the z direction
U, V, W	The relaxation variables
U_c	Entrainment flow velocity
x	Distance along the x direction
y	Distance along the y direction
$\frac{D}{Dt}$	Material derivative
Δ	Determinant
β	Entrainment coefficient
ϕ	Furrow bed sediment porosity
β_i	Eigen values for the jacobian of the flux matrix F
λ_i	Eigen values for the jacobian of the flux matrix G
ϵ	Relaxation parameter

$\nabla = \vec{i}\frac{\partial}{\partial x} + \vec{j}\frac{\partial}{\partial y} + \vec{k}\frac{\partial}{\partial z}$	Differential operator
$\prod$	Fluid viscosity
U'	Vector of conserved variables of the hydrodynamic component
$F'(U')$	Hydrodynamic component in the x direction
$G'(U')$	Hydrodynamic component in the y direction
$S'(U')$	The source term of the hydrodynamic component
ρ	Fluid density
ξ	Porosity of the furrow bed
ϕ	Total variation diminishing limiter function
$\frac{\partial F(U)}{\partial U}$	The Jacobian of the flux matrix F
$\frac{\partial G(U)}{\partial U}$	The Jacobian of the flux matrix G
MUSCL	Monotone Upstream Centred for the Conservation Laws
CFL	Courant-Friedrich's Courant condition
SWE	Shallow Water equations
CFD	Computational Fluid Dynamics

Abstract

In this work we apply a finite volume discretization technique based on a relaxation scheme to simulate the morphological evolution of the topography as a result of a dam break, that causes flooding downstream of the breach location. The considered mathematical model comprise of shallow water equations coupled with the bed updating equation which is modified to account for sediment entrainment process. Thus the model comprises a set of highly non-linear hyperbolic partial differential equations written in compact conservation form. In order to ensure that the resulting flux matrices are non-singular and are in compact conservation form, C-formulation was used. This formulation is an unsteady approach where the water flow and bed update are discretised simultaneously. The resulting Jacobian matrices could not be diagnolised easily and the eigenvalues were determined using the formulae for cubic functions as given by Spiegiel and Liu (1999). The non-linear partial differential equations written in C formulation were first relaxed into a set of linear hyperbolic system using the relaxation variables $\vec{V} = (V_1, V_2, V_3, V_4)\,, \vec{W} = (W_1, W_2, W_3, W_4)$. The relaxed equations were then discretized spatially (semi-discretization) using the Vanleer's MUSCL scheme which is total variation diminishing, and finally the time discretization (full discretization) was done using implicit-explicit Runge kutta scheme. The numerical model developed was used to simulate dam break flows and sediment transport on topographical surfaces with a deep narrow furrow and a topographic surface with two mounds located downstream of the breach location. Results on simulations showed that the entrainment and bed load transport significantly affected topography containing the furrow. The furrow widened and became shallower. Secondly the entrainment and the bed load sediment transport significantly affected the topography containing the two mounds. The mounds were eroded and there was high depositions of the sediments in the vicinity of the mounds and thirdly the dam break scenario with entrainment had a higher morphological evolution than the dam break scenario without the entrainment. The results thus obtained showed that the model is conservative, accurate, stable, robust, capable of resolving shocks and can handle even more complex geometries including simulations of real life dam break scenarios.

Chapter 1

INTRODUCTION

In this chapter the main terms used in this research are defined. In addition the objectives, significance and the hypothesis of this study are stated towards the end of the chapter.

1.1 Definition of terms

Definition 1.1.1. *(Shallow Water Equations)*

The Shallow Water Equations form a set of hyperbolic partial differential equations that describe the flow below the pressure surface in the fluid, sometimes but not necessarily, a free surface. The equations are derived from depth-integrating Navier-Stokes equations in the case where the horizontal length scale is much greater than the vertical length scale. The Shallow Water Equations are based on the assumption that over the flow depth the pressure distribution is hydrostatic. The waves are long i.e. wave lengths is much larger than the water depth $\frac{L}{h} > 20$*, in which the vertical acceleration of fluid elements during the wave passage stays small.*

Definition 1.1.2. *(Dam Break)*

This is the partial or catastrophic failure of a dam which leads to an uncontrolled release of water Fread (1993). When a semi-infinite water body initially at rest is released instantaneously by removal of a vertical barrier, such as in case of a dam failure, the resulting unsteady flow over a slopping or horizontal bed is termed as a dam break.

Definition 1.1.3. *(Soil Erosion)*

The catastrophic flooding as result a of a dam break leads to the soil erosion, the erosion can be described in three stages: detachment, transport and deposition. The detachment occurs when the flow shear stress or the kinetic energy of the flow exceeds the cohesive strength of the soil particles. Once detached, the sediments can be transported downstream as non-cohesive sediment before its deposition.

Definition 1.1.4. *(Sediment)*

The sediment can be defined as a fragmented material from rocks that has been formed by different physical and / or chemical process.

Definition 1.1.5. *(Entrainment)*

Entrainment is the process by which surface sediment is incorporated into a fluid flow (such as air, water or even ice) as part of the operation of erosion.

Definition 1.1.6. *(Sediment Transport)*

Sediment transport is divided into three types namely; bedload, saltation and suspension.

Bedload transport is defined as the type of transport where the sediments move in a layer close to the bottom of the topography and is characterized by a rolling and sliding movement.

Saltation transport is defined as the type of transport where single grains jump over the bed in length proportional to their diameter, loosing for instants the contact with the soil.

Suspended load is where the sediment is transported as a concentration of the water column and latter deposited in the bottom. Sediment is suspended when the flux is intense enough such as the sediments grains reach height over the bed. In this work we are interested with the bedload transport.

Definition 1.1.7. *(Conservative Forms)*

Equations such as Navier-Stokes equations commonly used in the modelling of ideal flows cannot be used to model real fluid flows in Eulerian differential form because they cannot be able to cater for the discontinuities. Where discontinuities occur in a solution the equations become meaningless because the derivative become undefined for the dependent variables. These discontinuities in a real flow describe hydraulic jumps, breaking waves, Tsunami (bore waves), and shocks in gas dynamics. However by re-writing the continuum equations into a conservation form, they can be generalized by use of integral formulation and will consequently hold for both continuous and discontinuous flows. Therefore numerical techniques for solving the equation set written in conservative form are desirable especially for dam-break flows.

Definition 1.1.8. *(Incompressible Flow)*

The conservation equations (3.63) assumes fluid and flow properties vary in time and space. In many applications fluid density is assumed constant while the compressibility is neglected in liquids. Such fluids are said to be incompressible.

Definition 1.1.9. *(Clapotis Gaufre)*

When waves interacts with an obstacle (mounds in our case) at a given angle, say β , the reflected waves will be directed off the structure at the same corresponding angle. The resulting wave motion is known as Clapotis Gaufre.

Definition 1.1.10. *(Consistency)*

Consistency means that the discrete equations approach (converge to) the differential equations for $\Delta x \to 0$, $\Delta y \to 0$ and $\Delta t \to 0$.

Definition 1.1.11. *(Convergence)*

The discrete solution U_1^n approaches the exact solution of the differential equation at every point $x_i = i\Delta x$, $y_j = j\Delta y$ and $t_n = n\Delta t$ if $\Delta x \to 0, \Delta y \to 0$ and $\Delta t \to 0$.

Definition 1.1.12. *(Stability)*

A stable difference scheme prevents the unlimited growth of numerical error during calculation.

Definition 1.1.13. *(CFL Condition)*

The Courant-Friedrichs-Lewy, (CFL condition) is a necessary condition for stability while solving hyperbolic PDEs numerically by the method of finite differences and finite volumes. It is a measure for the progress of a disturbance over a time step Δt. In two dimensions it has the form $C = \frac{u_x \Delta t}{\Delta x} + \frac{u_y \Delta t}{\Delta y} \leq C_{max}$ (with the obvious meaning of the symbols used).

1.2 Background Information

Water impoundments such as dams and water reservoirs are important part of any nation's infrastructure in both developed and developing countries. An

Figure 1.1: Chesbro dam and reservoir located in Llagas in Northern California . It can store 7945 acre-feet of water and has a surface area of 283 acres **Source**:www.valley.org/services/chesbrodam And Reservoir.aspx.

example is Kenya where as a matter of necessity every institution and even some homes have devised water storage mechanisms to cater for the time of need. The water impoundments are usually located in elevated positions in residential areas e.g the Chesbro dam (Fig 1.1). They provide good control mechanisms, water supply, irrigation, hydro-power, navigation and recreation benefits. On the contrary despite their many beneficial uses and value, they also present risks to property and life due to their potential to fail, and even cause catastrophic flooding. Some of the possible reasons responsible for a dam failure are large inflow into the reservoir, seepage or piping action through dam structure, embankment or slope failure, earthquake, landslides generated waves etc. Irrespective of the cause of failure, it is quite apparent that the elevated water waves rushing down can lead to massive destruction in the downstream reaches as shown in figure 1.2. Floods due to dam failure are generally significantly larger than natural floods as unexpected high peak in a very short duration and presence of a moving hydraulic shock/bore make it

a different problem as compared to other natural floods Singh (2005). The mitigation of the impacts of these possible risks, to the greatest possible degree requires modelling of the flood with sufficient detail so as to capture both the spatial and temporal evolution of the flood event. This therefore necessitates the need of devising an appropriate model which can correctly simulate effects of dam break failures, flood routing and sediment transport.

Figure 1.2: Flooding in Glashutte after the dam break in 12th August 2002
Source:http:espace.uq.edu.au/eserv/UQ:18350/chanson nova09.pdf.

1.3 Statement of the problem

Researchers have made significant contributions in the field of dam breaks and bed load sediment transport but majority of them used Godunov type methods in their simulations. Except Delis and Katsaounis (2005) who used the relaxation schemes developed by Jin and Xin (1995) which is simple, requires less computation time, achieves higher order accuracy and picks the right weak solutions, see Jin and Xin (1995). However in their work they did simulations of two mounds but in a confinement i.e the boundary conditions were all reflective and a breach was never considered . Therefore by considering a dam break

scenario as in our work, we simulate a situation that is more realistic. However this study was motivated by the work of the researchers Delis and Katsaounis (2005) and Simpson and Castelltort (2006) whereby the entrainment idea of Simpson and Castelltort (2006) and the two mounds idea of Delis and Katsaounis (2005) are combined to give more realistic simulations using the relaxation schemes. A further step is taken, which is to simulate morphological evolution of furrow located downstream of a breach location. Therefore in this work we apply a finite volume discretization technique based on a relaxation scheme to simulate the morphological evolution of the topography as a result of a dam break, that causes flooding downstream of the breach location. The considered mathematical model comprise of non-linear shallow water equations coupled with bed-updating equations which take into account the entrainment. The set of non-linear hyperbolic equations thus obtained are written in a compact conservation form. The numerical modelling is done using the finite volume, relaxation schemes. Using the relaxation approximation the non-linear hyperbolic equations are converted to a linear hyperbolic system using the relaxation variables $\vec{V} = (V_1, V_2, V_3, V_4), \vec{W} = (W_1, W_2, W_3, W_4)$. The spatial discretization is done using the Vanleer's Monotone Upstream Centered Scheme for Conservation Laws which is Time Variation Diminishing scheme, (MUSCL-TVD). The time discretization (Full discretization) was done using the implicit-explicit Runge-Kutta scheme. The capability of the model was tested by performing simulations of two different scenarios namely;

1. The morphological evolution of a topographic surface with a deep narrow furrow located downstream of the breach location.

2. The morphological evolution of a topographic surface with two mounds located downstream of the breach location.

1.4 Hypothesis

1. The 2-D Shallow water equations (SWE) are adequate in describing the considered flow problem.

2. The MUSCL-TVD method, a relaxation scheme despite being a Riemann-solver free method, achieves a second order accuracy and picks up the correct weak solutions in the solution of non-linear hyperbolic equations (in two-phase flow problem) as compared to Riemann or Godunov-type based methods which rely on approximate solutions of non-linear Riemann problem and only yields first order accuracy.

1.5 Objectives

1.5.1 General objective

To simulate the morphological evolution of the topography as a result of a dam break, that causes flooding downstream of the breach location.

1.5.2 Specific objectives

i.) To investigate effect of entrainment and bed-load transport on a topographic surface containing a narrow deep furrow after a dam break.

ii.) To investigate the effect of entrainment and bed-load transport on a topographic surface with two mounds located downstream of the dam break position.

1.6 Significance of the study

Dam break flows can cause serious flooding to downstream areas of the failed structures. Flood waves resulting from dam breaks have been responsible for severe losses of life and natural as well as man-made assets Hussain and Rai (2000). As a result, the prediction of dam break flows is an essential part of dam design, dam safety assessment, river flood control, water shed disaster mitigation etc. The quality of dam break flow prediction mainly depends on the appropriateness of mathematical formulation and the accuracy of numerical simulation models.

The correct prediction of local sediment transport in the vicinity of structures is an important research field due to its significant practical value as prediction is necessary for calculation of the scouring risk of the structures and the changes in the bed form. Several cases of the failure of structures exist where correct prediction of local scour was not done Hudson and Sweby (2003). Therefore accurate prediction of scour depth and its evolution in time is crucial. Sediment transport is an area of major interest to various professionals, for example the hydraulic engineers require this knowledge in the design of water ways. The understanding of how sand interacts with the water flow in certain environments such as coastal regions is also crucial to both the environment and business. For example, if a harbour is constructed such that a considerable amount of sand enters the harbour, the walls may become severely damaged

and the costs of dredging the harbour may become too expensive and almost impractical.

On the other hand sand can also be swept away from the beach resulting in only coarse sand remaining. This can result in a massive decline in tourists visiting the beach, and in turn severely affect the local community and businesses. Therefore in this research we endeavor to develop a numerical model which can possibly assist government agencies and other private institutions in conducting flood risk assessment studies, planning and designing flood control projects and establishing early warning systems and emergency actions.

1.7 Outline of the thesis

This thesis is organized into five chapters. Chapter two gives the literature review of the related work done by other researchers in the field of simulation of dam break flows and sediment transport on various channels. In chapter three equations governing the flow are modelled, they comprise of the shallow water equations and bed updating equations coupled with the entrainment. The shallow water equations are derived from continuity equation and momentum equations through the depth averaging and the long wave approximations. These equations form a set of a non-linear hyperbolic partial differential equations which are very difficult to solve analytically. Therefore a good choice of the method of solving these system of equations has been carefully done. The method chosen i.e. the relaxation method is robust, stable and accurately able to capture the location of discontinuities such as shocks and contact surfaces without using Riemann solvers. Unlike the relaxation scheme the Riemann solvers have a disadvantage in that it is time consuming requires a lot of

computer time. The relaxation method has simplicity and generality as its main feature, it uses neither Riemann solver spatially nor non-linear systems of algebraic equations solver temporally, yet it could achieve high order accuracy and picks up the right weak solutions.

In Chapter four, the equations are formulated using the C formulation, an unsteady approach which ensure that the Jacobian of the two flux matrices in the x and y directions are non-singular. The resulting characteristic equation is quite cumbersome and very difficult to solve because it contains several variables and therefore we adopt the formula for the cubic function as given by Spiegiel and Liu (1999). The relaxation is done by first converting the non linear hyperbolic equations to linear hyperbolic equations using the relaxation (artificial) valuables U, V, W. Spatial discretizations (semi-discretization) of the linear hyperbolic equations was done using the Vanleer's MUSCL-TVD method, while the time discretization (full discretization) was done using the fourth order implicit-explicit Runge-Kutta method.

Chapter five presents the results and the discussion of the research problem, it is divided in four sections. Section one presents the initial and the boundary conditions governing the research problem. In section two we present and discuss the results for the effect of entrainment, morphological evolution and bedload transport on the topographic surface having a narrow deep furrow. The water depth contours, velocity vector plots, furrow profiles at three different time intervals and the aerial view of the topographic surface before and after morphological evolution have been presented. Section three provides the results for the effect of entrainment, morphological evolution and the bed load

transport on a topographic surface having two mounds downstream of the breach location. In this section we have presented the water depth contours, the vector velocity plots and the aerial view of the topographic surface before and after morphological evolution the two mounds. While in section four the conclusion of this study and the recommendations for future research works are presented.

.

Chapter 2

LITERATURE REVIEW

In this chapter we give an account of the related work which has been done on simulation of dam break flows and sediment transport along the channels. Zoppou and Stephen (1991) presented their work on catastrophic collapse of water supply reservoirs in urban areas. In their study they developed a model based on finite volume method combined with a first order approximate Riemann solver to solve the two-dimensional shallow water wave equation on an unstructured triangular grid. The model was applied to a case study involving the sudden collapse of a water supply reservoir to predict the progress of the flood ensuing from an instantaneous collapse of the reservoir. The model was found to be conservative, robust, efficient, and capable of simulating wetting and drying processes, resolving shocks, simulating flows around complex geometries, and obstacles including influence of steep bed slopes and friction.

Zhou *et al.* (2004) presented their work on numerical prediction of dam-break flows in general geometries with complex bed topography. In their work

they did numerical simulations of dam break flows in general geometries with complex bed topography using a high-resolution Godunov-type cut cell method. The model was based on shallow water equations with appropriate source terms. A vertical step in the bed was treated efficiently and accurately with the surface gradient method (SGM). For dam-break flows occurring in complicated geometries, the Cartesian cut cell method together with transmissive boundary conditions were incorporated. Verification of the model was carried out by predicting dam-break flows typical of practical situations, i.e. dam break flows over a vertical step into bent channels and a dam break flow over a bump in bed with both transmissive and reflective boundary conditions at the channel end. The results were compared with experimental data and showed good agreement.

Biscarini *et al.* (2010) presented their work on numerical simulations of free surface flows induced by a dam break comparing the shallow water approach to fully three-dimensional simulations. The three-dimensional simulations were based on the solution of the complete set of Reynolds-Averaged Navier-Stokes (RANS) equations coupled to the volume of fluid (VOF) method. The methods assessment and comparison were carried out on three scenarios namely a dam break over a flat bed without friction, a dam break over a triangular bottom sill and a dam break flow over a 90^0 bend. The results showed that the shallow water approach though was sufficiently able to reproduce the main aspects of the fluid flows, loses some three- dimensional phenomena, due to the incorrect shallow water idealization that neglects the three-dimensional aspects related to the gravity force.

Singh *et al.* (2011) developed a two-dimensional numerical modelling of dam-break flows over natural terrain using a central explicit scheme. The governing equations were modelled using the shallow water equations, the spatial derivatives were discretized using a well-balanced explicit central upwind conservative scheme while the time integration was performed using the Euler's scheme. The model was validated by simulating a laboratory experiment in which a dam break flow propagates over a triangular obstacle and the model was found to be satisfactory. A dam case laboratory experimental test case on a friction-less horizontal bottom was also simulated for the 2-D validation of the model, and a good agreement between simulation and experimental data was observed. The suitability of the model for real life applications was demonstrated by simulating the Malpasset dam-break event which occurred in France in 1959. The computed arrival time of flood wave front and maximum flow depths at various observation points matched well with the measurements on a $\frac{1}{400}$ physical scale model.

The overall performance indicated that the model could be applied for simulation of dam break flows in real life situation. Lachouette *et al.* (2009) presented their work on a numerical modelling of Interfacial soil erosion. In their study they developed a numerical model for simulating the surface tension occurring at a fluid/soil interface undergoing a flow process. The balance equations with jump relations were used. A penalization procedure was used to compute Stokes's equations around obstacles, with a fictitious domain method, in order to avoid body-fitted unstructured meshes and to use fast and efficient finite volumes approximations on Cartesian meshes. The water/soil interface

evolution was described with a Level Set function. The ability of the model to predict the interfacial erosion of soils was confirmed by presenting several 2-D simulations.

Ahmad *et al.* (2013) presented their work on numerical method for dam break problem by using Godunov approach. They developed a numerical scheme in order to overcome the problem of shock waves for the test case of a dam break problem in one and two dimensions. The numerical scheme was based on Godunov approach of finite volume method to solve the shallow water equations. In order to expedite and improve the solution an approximate Roe's Riemann solver associated with monotone Upstream Centered Scheme for Conservation Laws was applied. The results were presented in one and two dimensions and verification were made with analytical solution. The results were comparable and a good agreement was achieved between numerical and analytical.

Audusse *et al.* (2013) presented their work on parallelization of a relaxation scheme, modeling the bed load transport of sediments in shallow water. They did numerical simulations for bed load erosion processes. In their work they presented a relaxation solver that could be applied to moving dunes test cases in one and two dimensions which was not easy to handle at numerical level especially when soft coupling (i.e. independent solvers or fluid and solid parts). To run $2D$ test cases with reasonable CPU time they applied a parallelization procedure by using domain decomposition based on the classical MPI library. Brufao *et al.* (2002) studied a numerical model for the flooding and drying

of irregular domains. In their work they developed a numerical technique for the modelling of shallow water flow in one and two dimensions. The model comprised of a cell-centered finite volume method based on Roe's approximate Riemann solver across the edges of both structured and unstructured cells. The discretization of the bed slope source terms was done using an upwind approach. The model was tested in different applications involving unsteady flows in complex geometries such as dam break and advance over a triangular obstacle, propagation of a smooth wave over a bump, non-symmetric dam break in a pool with a pyramidal obstacle. The real life application was done by simulating propagation of a flood wave in the Toce river physical model. These results were validated with the successful comparison between the numerical results and the experimental data.

Brufao and Navarro (2003) studied unsteady free surface simulation over complex topography with a multidimensional upwind technique. They developed a numerical model based on a first order upwind technique to solve one-and two-dimensional problems for steady and unsteady free surface flows. The model was tested in different applications involving unsteady flows in complex geometries such as steady flow over a bump, dam break through a trapezoidal breach, dam break in converging-diverging channel and steady flow in three bumps. This numerical technique was validated with the successful comparison between the numerical results and the experimental data.

Jean-Marie and Azzeddine (2010) presented a multi-dimensional upwind scheme modelling wetting-drying transitions in free surface flows over complex

topographies. They proposed a 2-D cell centered finite-volume scheme for solving shallow water equations using both structured and unstructured fixed meshes. Steady state C property and global mass conservation properties were satisfied using appropriate numerical fluxes and wet/dry surface treatments. The model was tested in different applications including idealized 1-D dam break flow problems, Dam break on wet flat bottom, Dam break on dry flat bottom and vacuum test with two expansion waves. The model was also applied on a real case of wetting-drying simulations in a portion of the river "Riviere des prairies" in a suburb of Laval Quebec. With these validations the model was found to be stable and robust.

Singh (2005) presented a two dimensional sediment transport model using parallel computer that is, a vertically integrated two-dimensional numerical sediment transport model. The sediment transport was simulated in two parts namely, suspended load and bed load. He used the fractional step approach to solve the two dimensional advection-diffusion equation which splits the advection-diffusion equation in two separate parts i.e. advection and diffusion. To solve advection part he used the high resolution conservative algorithm and semi-implicit finite difference scheme to solve the diffusion part. To solve the linear system of equations resulting from different diffusion part, parallel numerical solvers were developed. He made the observation that the model could simulate suspended load and bed load separately and that the bed load transport is sensitive to different bed load transport capacity formulas and hence he cautioned that care be taken in choosing the bed load transport

capacity formula.

Brufao *et al.* (2004) developed a 2D numerical model for dam break flows and achieved a zero mass error by modifying the wetting-drying condition which included the normal velocity to the cell edges. Hudson and Sweby (2003) investigated an accurate numerical solution of the equations governing bed-load sediment transport. In their work they considered two approaches of sediment flow namely the steady and unsteady approaches and compared the accuracy of the formulations within their frameworks. They observed that the formulation $A - CV$ in the steady approach produced the most accurate results though only to some limited values of the dimensional constant, A and the sediment transport flux q. Of the two approaches the unsteady approach formulations were found to be more accurate than the steady approach and on overall formulation C was found to be the most accurate as B could not handle shocks in the cases of discontinuous flows. They observed that steady approaches worked best when the Froude number, Fr is small and when the bed interacts slowly with the water flow while the unsteady approaches could be used for all values of the dimensional constant A and the Froude number Fr.

Jin and Levermore (1996) studied numerical schemes for hyperbolic conservation laws with stiff source terms and showed through asymptotic analysis and numerical examples that semi-discrete high resolution methods for hyperbolic conservation laws fail to capture the asymptotic behavior unless the small relaxation rate is reserved by a fine spatial grid. They introduced a modification of high- order Godunov methods that possess the correct asymptotic behavior

allowing the use of coarse grids (large cell peclets number).

Jin and Xin (1995) presented for the first time a new class of numerical scheme known as the relaxation schemes for a system of conservation laws in several space dimensions. They used a local relaxation approximation to construct a linear hyperbolic system with a stiff lower order term that approximates the original system with a small dissipative correction. Unlike the then popular Godunov schemes such as upwind methods and central schemes which relied on approximate solutions of non-linear Riemann problems, the new linear hyperbolic system was solved by under-resolved stable numerical discretizations, without using either Riemann solvers spatially or a non-linear system of algebraic equation solvers temporally, yet it achieved high order accuracy and picked the right weak solutions. The numerical results obtained showed that the second order schemes are total variation diminishing (TVD) in the zero relaxation limit for scalar equations.

Chalabi (1999) studied the convergence of relaxation schemes for hyperbolic conservation laws with stiff source terms. He presented an analysis of a class of relaxation schemes for hyperbolic conservation laws including stiff source terms which had been introduced earlier, see Jin and Xin (1995) as explained above in this literature. The construction of these schemes were based on the approximation of an associated linear hyperbolic system with a stiff source term depending on a small parameter ϵ called relaxation time. This method avoided the use of Riemann-solvers, and with an adequate and realistic hypothesis, $(q'(u) \leq 0)$ on the source term $q(u)$ that is with a dissipative source $q(u)$,

proposed semi-implicit and fully-implicit numerical schemes possessing good properties such as monotony, TVD character, etc., exactly as in the case of conservation laws without a source term $q = 0$ and showed that under reasonable CFL conditions, the convergence of the approximate solution toward a weak solution or to the entropy satisfying solution was established.

Delis and Katsaounis (2003) investigated a finite difference method for calculating numerical solutions of the two dimensional shallow water systems with source term based on bed topography. The method was based on classical relaxation models combined with the TVD Runge-Kutta time stepping mechanism where neither Riemann solvers nor characteristics decomposition were used. The numerical results were presented for several test problems with or without the the source term present. They observed that the method had numerical dissipation especially while preserving steady states.

Delis and Katsaounis (2005)presented their work on the numerical solution of two-dimensional shallow water equations by the application of relaxation methods. They investigated a generalization and extension of a finite difference method for calculating numerical solutions of the two dimensional shallow water system of equations with source terms. The methods were based on classical TVD Runge-Kutta time stepping mechanism where neither Riemann solvers nor characteristics decomposition were needed. The presented numerical results for several test problems with or without the source terms present such as 2-D partial dam break, circular dam break, steady flow over a hump, and a dam break in a channel with topography and friction. The bench mark tests

showed that the relaxation schemes provide accurate solutions which were in good agreement with well documented ones and besides having a comparable resolutions with other well established methods they have simplicity as their core advantage. This work was an improvement of his earlier work but this time they devised novel ways of incorporating source terms with only small errors being introduced while preserving steady states.

Diaz *et al.* (2008) presented their work on Sediment transport models in shallow water equations and numerical approach by high order finite volume methods. In their work they focused on numerical approximation of bed load transport due to water evolution and came up with a coupled model consisting of hydrodynamic component and morphodynamic component. This model was a set of non-conservative hyperbolic system of equations which were then solved numerically using finite volume methods. These results were compared with analytical solutions and experimental data and showed a good agreement.

Simpson and Castelltort (2006) presented a coupled model of surface water flow, sediment transport and morphological evolution. The model was based on shallow water equations for flow, conservation of sediment concentration, and empirical functions for bed friction, substrate erosion and deposition. The resulting hyperbolic system was solved using finite volume, Godunov-type method with a first-order approximate Riemann solver. The developed model could be used to investigate a variety of problems involving coupled flow and sediment transport including channel initiation and drainage basin evolution associated with overland flow and morphological changes induced by extreme

events such as tsunami.

From the cited literature review which has given an account of the contributions in the field of dam breaks and sediment transport it is clear that majority of researchers used Godunov type methods in their simulations, except Delis and Katsaounis (2005) who used the relaxation schemes developed by Jin and Xin (1995) which is simple, requires less computation time, achieves higher order accuracy and picks the right weak solutions, see Jin and Xin (1995). However in their work they did simulations of two mounds but in a confinement i.e reflective boundaries and they never considered a breach. Therefore by considering a dam break scenario as in our work, we simulate a situation that is more realistic. However this study was motivated by the work of the researchers Delis and Katsaounis (2005) and Simpson and Castelltort (2006) whereby the entrainment idea of Simpson and Castelltort (2006) and the two mounds idea of Delis and Katsaounis (2005) are combined to give more realistic simulations using the relaxation schemes. A further step is taken, which is to simulate morphological evolution of furrow located downstream of a breach location.

Chapter 3

THE GOVERNING EQUATIONS

In this chapter we develop a mathematical model for a dam break and sediment transport. This model is developed by coupling morphodynamic component and hydrodynamic components. The hydrodynamic component is modeled by shallow water equations while the morphodynamic component is modeled by bed updating equation coupled with entrainment.

3.1 Derivation of Shallow Water equations

In this section we derive the shallow water equations with source terms due to bed topography, frictional forces and entrainment. These equations are derived from the principles of conservation of mass and conservation of momentum. The independent variables are time t, and two space co-ordinates x and y, while the dependent variables are the fluid height or depth h and the 2-dimensional fluid flow rates, hu and hv. With the proper choice of units,

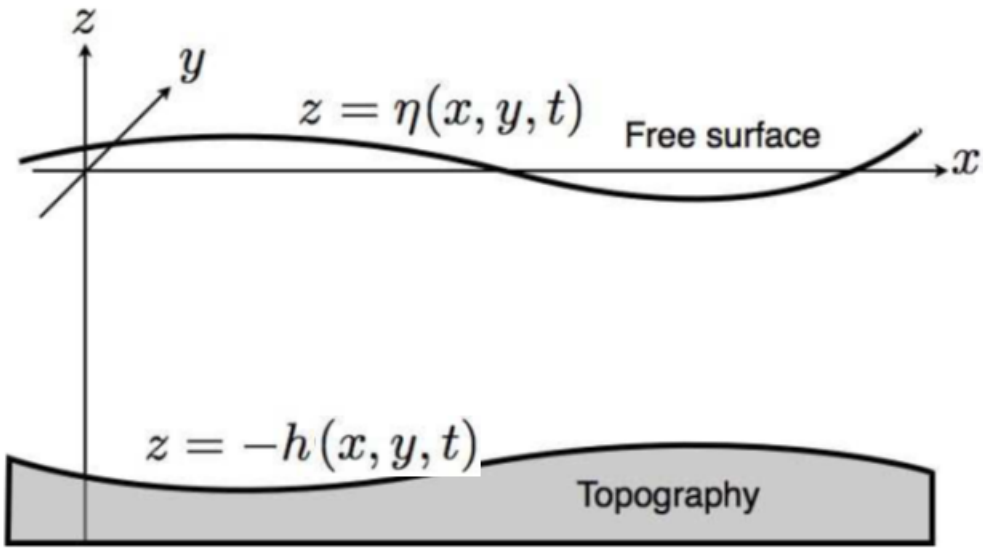

Figure 3.1: The Free surface Flow

the conserved quantities are mass, which is proportional to h, and momentum which is proportional to u and v. The force acting on the fluid is gravity represented by the gravitational constant g. The underlying assumption in the derivation of these equations is that the depth of the fluid is small compared to wave length of the disturbance. Since shallow water equations describe a thin layer of fluid of constant density in hydrostatic balance, bounded from below by bottom topography and above by a free surface the appropriate boundary conditions will be stated and applied accordingly in the derivation of these equations.

3.1.1 The conservation of Mass

This equation is based on two fundamental propositions:

i.) That the mass of the fluid is conserved i.e. it can neither be created nor destroyed

ii.) The flow is continuous and that empty spaces do not occur between particles which were in contact

In differential form it is given as;

$$\frac{\partial \rho}{\partial t} + \nabla \cdot (\rho \vec{V}) = 0 \tag{3.1}$$

where ρ is the density and $\vec{V} = (u, v, w)$ is the velocity.

For an incompressible fluid (there is no variation of density with pressure). Also, salinity and temperature can be assumed as constant. So fluid density, ρ is constant in all the domain. Equation (3.1) becomes;

$$\nabla \cdot \vec{V} = 0 \tag{3.2}$$

The equation (3.2) may be expressed as continuity equation. In differential form in $3 - D$ flow it takes the form;

$$\frac{\partial u}{\partial x} + \frac{\partial v}{\partial y} + \frac{\partial w}{\partial z} = 0 \tag{3.3}$$

3.1.2 The Conservation of Momentum

Newton's second law of motion is used to derive the equation of conservation of momentum Anderson *et al.* (1984), in differential form the equation is given as;

$$\frac{\partial (\rho \vec{V})}{\partial t} + \nabla \cdot \left[\rho \vec{V} \otimes \vec{V} + PI - \prod \right] = \rho g \tag{3.4}$$

where $\vec{V}$ is the velocity, ρ is the density, P is the pressure, $\prod$ is the viscosity of the fluid and g is the body force vector. Assuming that water is inviscid

then $\prod = 0$ and the equation (3.4) becomes ;

$$\frac{\partial(\rho\vec{V})}{\partial t} + \nabla \cdot \left[\rho\vec{V} \otimes \vec{V} + PI\right] = \rho g \tag{3.5}$$

Since the fluid considered is incompressible then the equation (3.5) takes the form;

$$\frac{\partial\vec{V}}{\partial t} + \nabla \cdot \left[\vec{V} \otimes \vec{V}\right] + \frac{1}{\rho}\nabla \cdot PI = g \tag{3.6}$$

Now adopting the convention that the horizontal plane is given by the coordinates x and y and the vertical direction by z and also by denoting the components of the body force vectors by $g = (g_1, g_2, g_3)$=(0,0,-g) where g is the acceleration due to gravity (assumed constant). Then the equation (3.6) becomes

$$\frac{\partial\vec{V}}{\partial t} + \nabla \cdot \left[\vec{V} \otimes \vec{V}\right] + \frac{1}{\rho}\nabla \cdot PI = \begin{bmatrix} 0 \\ 0 \\ -g \end{bmatrix} \tag{3.7}$$

Rearranging equation (3.7), it takes the form

$$\frac{\partial\vec{V}}{\partial t} + \nabla \cdot \left[\vec{V} \otimes \vec{V}\right] = -\frac{1}{\rho}\nabla \cdot PI + \begin{bmatrix} 0 \\ 0 \\ -g \end{bmatrix} \tag{3.8}$$

Equation (3.8) can be expressed in a more simplified form as;

$$\begin{aligned}
\frac{\partial u}{\partial t}+u\frac{\partial u}{\partial x}+v\frac{\partial u}{\partial y}+w\frac{\partial u}{\partial z} &= -\frac{1}{\rho}\frac{\partial p}{\partial x}\\
\frac{\partial v}{\partial t}+u\frac{\partial v}{\partial x}+v\frac{\partial v}{\partial y}+w\frac{\partial v}{\partial z} &= -\frac{1}{\rho}\frac{\partial p}{\partial y}\\
\frac{\partial w}{\partial t}+u\frac{\partial w}{\partial x}+v\frac{\partial w}{\partial y}+w\frac{\partial w}{\partial z} &= -\frac{1}{\rho}\frac{\partial p}{\partial z}-g
\end{aligned} \tag{3.9}$$

3.1.3 Boundary conditions

The mass continuity equation (3.3) and the conservation of momentum equations (3.9) constitute the four equations with four unknowns i.e u, v, w and p which by applying the appropriate boundary conditions may be solved as spatial functions of x, y, z and time t.

The shallow water equations are approximations to free surface problem of the figure 3.1. The boundary conditions for the free surface under gravity $Z = \eta(x, y, t)$ and the bottom surface $Z = -B(x, y)$ are respectively;

$$\frac{D}{Dt}(\eta - Z) = 0 \tag{3.10}$$

$$p = p_{atm}, \tag{3.11}$$

where p_{atm} is the atmospheric pressure. At the bottom we have;

$$\frac{D}{Dt}(B + Z) = 0, Z = -B(x, y) \tag{3.12}$$

we also impose the no-slip condition at the bottom;

$$u = v = 0 \tag{3.13}$$

Expanding the boundary conditions (3.10) we obtain;

$$(\eta_t + u\eta_x + v\eta_y - w)\,|_{z=\eta} = 0 \tag{3.14}$$

Expanding the boundary condition (3.12) in a similar way we get;

$$(uB_x + vB_y + w)\,|_{z=-B} = 0 \tag{3.15}$$

3.1.4 Boundary Layer Theory

The primary assumption in shallow water theory is that the horizontal scales having wave length L are much larger than the vertical scales (in an undisturbed water height).

We now analyse the equation of mass (3.3) as shown below;

$$\underbrace{\frac{\partial u}{\partial x} + \frac{\partial v}{\partial y}}_{\approx \frac{u}{l}} + \underbrace{\frac{\partial w}{\partial z}}_{\approx \frac{w}{h}} = 0 \tag{3.16}$$

and we deduce that

$$w \approx u\frac{h}{l} \tag{3.17}$$

Where $\frac{h}{l} \ll 1$ and this leads to a boundary layer assumption;

$$\frac{\partial w}{\partial t} = 0 \tag{3.18}$$

Now neglecting the vertical accelerations the system of equations (3.9) takes the form;

$$\begin{aligned} \frac{\partial u}{\partial t} + u\frac{\partial u}{\partial x} + v\frac{\partial u}{\partial y} + w\frac{\partial u}{\partial z} &= -\frac{1}{\rho}\frac{\partial p}{\partial x} \\ \frac{\partial v}{\partial t} + u\frac{\partial v}{\partial x} + v\frac{\partial v}{\partial y} + w\frac{\partial v}{\partial z} &= -\frac{1}{\rho}\frac{\partial p}{\partial y} \\ \frac{\partial w}{\partial t} &= -\frac{1}{\rho}\frac{\partial p}{\partial z} - g \end{aligned} \tag{3.19}$$

and now applying the boundary layer assumption equation (3.18) unto equation (3.19) we get;

$$\begin{aligned} \frac{\partial u}{\partial t} + u\frac{\partial u}{\partial x} + v\frac{\partial u}{\partial y} + w\frac{\partial u}{\partial z} &= -\frac{1}{\rho}\frac{\partial p}{\partial x} \\ \frac{\partial v}{\partial t} + u\frac{\partial v}{\partial x} + v\frac{\partial v}{\partial y} + w\frac{\partial v}{\partial z} &= -\frac{1}{\rho}\frac{\partial p}{\partial y} \\ 0 &= -\frac{1}{\rho}\frac{\partial p}{\partial z} - g \end{aligned} \tag{3.20}$$

3.1.5 Hydrostatic Pressure

The vertical component of equation (3.20) can be re-written as;

$$\frac{\partial p}{\partial z} = -\rho g \tag{3.21}$$

integrating equation (3.21) with respect to z we get the following hydostatic pressure relation;

$$p = g \int_z^\eta \rho dz + p_a \tag{3.22}$$

Assuming constant density along the z axis the equation (3.22) becomes;

$$p = \rho g \left(\eta - z\right) + p_a \tag{3.23}$$

Differentiating equation (3.23) with respect to x we get the pressure gradient along the x direction as;

$$\frac{\partial p}{\partial x} = \rho g \frac{\partial \eta}{\partial x} \tag{3.24}$$

Similarly, differentiating the same equation (3.23) with respect to y we get the pressure gradient along the y direction as;

$$\frac{\partial p}{\partial y} = \rho g \frac{\partial \eta}{\partial y} \tag{3.25}$$

and hence from the equations (3.24) and (3.25), it's clear that the hydrostatic pressure relation (3.22) is independent of the variable z and therefore it is only responsible for the horizontal accelerations;

3.1.6 Horizontal Mean Velocity

The horizontal velocities u and v are independent of the variable z and can be interpreted as the vertical mean velocities and therefore can be written in the form;

$$\frac{\partial u}{\partial z} = \frac{\partial v}{\partial z} = 0 \tag{3.26}$$

3.1.7 The simplified Momentum Equations

Putting equation (3.24) and (3.26) in the first of the equations (3.20), equation (3.25) and (3.26) in the second of the equation (3.20) we get the following set of equations;

$$\frac{\partial u}{\partial t} + u\frac{\partial u}{\partial x} + v\frac{\partial u}{\partial y} = -g\frac{\partial \eta}{\partial x} \tag{3.27}$$

$$\frac{\partial v}{\partial t} + u\frac{\partial v}{\partial x} + v\frac{\partial v}{\partial y} = -g\frac{\partial \eta}{\partial y} \tag{3.28}$$

3.1.8 Depth Averaging

Now integrating the continuity equation vertically;

$$\int_{-B}^{\eta} \nabla \cdot \vec{V} dz = 0, -B < Z < \eta \tag{3.29}$$

Expanding the continuity equation, we get;

$$0 = \int_{-B}^{\eta} \left[\frac{\partial u}{\partial x} + \frac{\partial v}{\partial y} + \frac{\partial w}{\partial z}\right] dz \tag{3.30}$$

. We now apply the Leibintz rule of integration to integrate equation (3.30), we obtain;

$$\begin{aligned} 0 &= \frac{\partial}{\partial x}\int_{-B}^{\eta} u dz - u|_{z=\eta}\frac{\partial \eta}{\partial x} + u|_{z=-B}\frac{\partial(-B)}{\partial x} \\ &+ \frac{\partial}{\partial y}\int_{-B}^{\eta} v dz - v|_{z=\eta}\frac{\partial \eta}{\partial y} + v|_{z=-B}\frac{\partial(-B)}{\partial y} \\ &+ w|_{z=\eta} - w|_{z=-B} \end{aligned} \tag{3.31}$$

And now putting (3.15) into (3.31) the above equation becomes;

$$\begin{aligned} 0 &= \frac{\partial}{\partial x}\int_{-B}^{\eta} u dz - u|_{z=\eta}\frac{\partial \eta}{\partial x} \\ &+ \frac{\partial}{\partial y}\int_{-B}^{\eta} v dz - v|_{z=\eta}\frac{\partial \eta}{\partial y} \\ &+ w|_{z=\eta} \end{aligned} \tag{3.32}$$

Now applying the boundary conditions (3.14) to the equation (3.32) we get;

$$\frac{\partial \eta}{\partial t} + \frac{\partial}{\partial x}\int_{-B}^{\eta} u dz + \frac{\partial}{\partial y}\int_{-B}^{\eta} v dz = 0 \tag{3.33}$$

. Since u and v are independent of z then the equation (3.33) becomes;

$$\frac{\partial \eta}{\partial t} + \frac{\partial[(\eta + B)u]}{\partial x} + \frac{\partial[(\eta + B)v]}{\partial y} = 0 \tag{3.34}$$

. Assuming that in this particular case that $B(x, y)$ is independent of time then it implies that $B_t = 0$ and therefore we can write the equation (3.34) as;

$$(\eta + B)_t + [u(\eta + B]_x + [v(\eta + B)]_y = 0 \tag{3.35}$$

Now multiplying the equation (3.35) by u and adding to equation (3.27) pre-multiplied by $(\eta + B)$, we obtain;

$$[u\,(\eta + B)]_t + [u^2(\eta + B]_x + [uv(\eta + B)]_y = -g(\eta + B)\eta_x \tag{3.36}$$

Similarly multiplying equation (3.35) by v and then add to the equation (3.28) pre-multiplied by $(\eta + B)$ we obtain;

$$[v\,(\eta + B)]_t + [uv(\eta + B]_x + [v^2(\eta + B)]_y = -g(\eta + B)\eta_y \tag{3.37}$$

The right hand side of equation (3.36) can be expanded as follows;

$$-\,g(\eta + B)\eta_x = g(\eta + B)B_x - \frac{1}{2}g[(\eta + B)^2]_x \tag{3.38}$$

Expanding the right hand side of equation (3.37) we obtain;

$$-\,g(\eta + B)\eta_y = g(\eta + B)B_y - \frac{1}{2}g[(\eta + B)^2]_y \tag{3.39}$$

Putting $(\eta + B) = h$ where h is the total water height then the equation (3.35) takes the form;

$$h_t + (hu)_x + (hv)_y = 0 \tag{3.40}$$

Again letting $(\eta + B) = h$ and expanding the right hand side of the equation according to (3.36) we obtain;

$$(hu)_t + (hu^2 + \frac{1}{2}gh^2)_x + (huv)_y = -ghB_x \tag{3.41}$$

Similarly expanding the right hand side of the equation (3.37) while letting $(\eta + B) = h$ we obtain;

$$(hv)_t + (huv)_x + (hv^2 + \frac{1}{2}gh^2)_y = -ghB_y \tag{3.42}$$

3.1.9 The Final form of Shallow Water Conservation Equations (Hydrodynamics Equations)

The equation of continuity (3.40) and the equations of the conservation of momentum (3.41) and (3.42) combined together form a set of system of equations in conservation form;

$$\begin{aligned} h_t + (hu)_x + (hv)_y &= 0 \\ (hu)_t + (hu^2 + \frac{1}{2}gh^2)_x + (huv)_y &= -ghB_x \\ (hv)_t + (huv)_x + (hv^2 + \frac{1}{2}gh^2)_y &= -ghB_y \end{aligned} \tag{3.43}$$

where h is the height of the water, u and v are the depth averaged velocities in the x and y directions respectively and $B = B(x, y)$ is the function describing the bottom profile. We can now express the system of shallow water equations (3.43) in a more compact conservation form as follows;

$$U'_t + F'(U')_x + G'(U')_y = S'(U') \tag{3.44}$$

where;

$U' = [h, hu, hv]^T$ is the vector of the conserved variables,

$F'(U') = [hu^2, hu^2 + \frac{1}{2}gh^2, huv]^T$ is the flux in the x direction

$G'(U') = [hv, huv, hv^2 + \frac{1}{2}gh^2]^T$ is the flux in the y direction

and

$S'(U') = [0, -ghB_x, -ghB_y]^T$ is the source term

3.1.10 Bed-updating Equation

When deriving this equation, we assume that height of the river bed denoted by B , is not stationary. We therefore express it as function of the space coordinates x, y and time t i.e

$$B = B(x, y, t) \tag{3.45}$$

and take the boundary condition as;

$$\frac{D}{Dt}(Z - B) = 0 \tag{3.46}$$

. Now using the definition of the material derivative we can expand the boundary condition (3.46) as follows;

$$B_t + uB_x + vB_y - w|_{z=B} = 0 \tag{3.47}$$

. Integrating the bed-update equation vertically we get;

$$\int_0^B \nabla \cdot \vec{V} dz = 0 \tag{3.48}$$

. Expanding the equation (3.48), we write it as;

$$\int_0^B \left[\frac{\partial u}{\partial x} + \frac{\partial v}{\partial y} + \frac{\partial w}{\partial z}\right] dz = 0 \tag{3.49}$$

. Integrating equation (3.49) using the Leibntz rule we get;

$$\begin{aligned} 0 &= \frac{\partial}{\partial x}\int_0^B u dz - u|_{z=B}\frac{\partial B}{\partial x} \\ &+ \frac{\partial}{\partial y}\int_0^B v dz - v|_{z=B}\frac{\partial B}{\partial y} + v_{z=B}\frac{\partial\,(B)}{\partial y} \\ &+ w|_{z=B} - w|_{z=0} \end{aligned} \tag{3.50}$$

Substituting the expanded boundary condition (3.47) to equation (3.50), we get;

$$B_t + \frac{\partial}{\partial x}\int_0^B u dz + \frac{\partial}{\partial y}\int_0^B v dz = 0 \tag{3.51}$$

Equation (3.51) may be expressed in the form;

$$B_t + \frac{\partial}{\partial x}(Bu)dz + \frac{\partial}{\partial y}(Bv)dz = 0 \tag{3.52}$$

The volumetric load transport in x and y directions according to (Kaushik 2005) is respectively expressed as;

$$Bu = \xi p_1 \tag{3.53}$$

$$Bv = \xi p_2 \tag{3.54}$$

Where;

$\xi = \frac{1}{1-\epsilon}$ and ϵ is the porosity of the furrow

Now putting (3.53) and (3.54) into equation (3.52), we get the bed updating equation;

$$\frac{\partial}{\partial t}B + \xi\frac{\partial}{\partial x}(p_1) + \xi\frac{\partial}{\partial y}(p_2) = 0 \tag{3.55}$$

In our case we are interested with the bed load sediment transport and its effects such as entrainment on various topographies. Various scientist have come up with numerous analytical sediment transport formula of which the choice depends on the particular situation being modeled. In our work we shall adopt the one derived by Grass (1981) because it is a simple model and the critical shear stress is set to zero;

$$p_1 = Au(u^2 + v^2)^{\frac{m-1}{2}} \tag{3.56}$$

$$p_2 = Av(u^2 + v^2)^{\frac{m-1}{2}} \tag{3.57}$$

Where A is a dimensional constant $\frac{s^2}{m}$,(where s is the specific gravity) which encompasses the effects of the grain size and kinematic viscosity which is being chosen from an experimental data. We observe that the equations (3.56) and (3.57) can only be differentiated with respect to u and v respectively only if they are not allowed to change signs.

However, by considering the odd integers of m only then the equations (3.56) and (3.57) can be differentiated and become valid for all values of u and v and hence for this reason we shall use the value of $m = 3$ as it is the smallest convenient odd integer which maintains postivity.

3.1.11 The Final form of the Governing Equations (Morphodynamic Equations)

In this research we shall adopt the following formula for entrainment as given by Simpson and Castelltort (2006);

$$E' = \beta \left[\frac{\sqrt{(u^2 + v^2)}}{u_c} - 1 \right]^{\gamma} \tag{3.58}$$

Where β is the entrainment coefficient, u_c is a threshold entrainment flow velocity (Izumi and Parker 2000)and therefore the continuity equation becomes;

$$h_t + (hu)_x + (hv)_y = \frac{E'}{1-\phi} \tag{3.59}$$

. Similarly the updating equation becomes;

$$\frac{\partial}{\partial t} B + \xi \frac{\partial}{\partial} p_1 + \xi \frac{\partial}{\partial} p_2 = \frac{E'}{1-\phi} \tag{3.60}$$

where ξ is the bed sediment porosity. Now considering the effects of the friction on the x and y directions and incorporating in momentum equations, we get;

$$(hu)_t + (hu^2 + \frac{1}{2} g h^2)_x + (huv)_y = -ghB_x - ghS_{fx} \tag{3.61}$$

$$(hv)_t + (huv)_x + (hv^2 + \frac{1}{2} g h^2)_y = -ghB_y - ghS_{fy} \tag{3.62}$$

Now coupling the derived shallow water equations to the equations for the sedimentation of mass we now come up with final equations governing the

sediment transport.

$$\begin{aligned} h_t + (hu)_x + (hv)_y &= \frac{E'}{1-\phi} \\ (hu)_t + \left(hu^2 + \frac{1}{2}gh^2\right)_x + (huv)_y &= -ghB_x - ghS_{fx} \\ (hv)_t + (huv)_x + \left(hv^2 + \frac{1}{2}gh^2\right)_y &= -ghB_y - ghS_{fy} \\ \frac{\partial}{\partial t}B + \xi\frac{\partial}{\partial x}(p_1) + \xi\frac{\partial}{\partial y}(p_2) &= \frac{E'}{1-\phi} \end{aligned} \tag{3.63}$$

where the friction forces in the two respective direction is as given by the Darcy-Weisbach equation;

$$S_{fx} = \frac{fu\sqrt{u^2+v^2}}{8gh}, S_{fy} = \frac{fv\sqrt{u^2+v^2}}{8gh} \tag{3.64}$$

where t is the time, x and y are horizontal coordinates, h is the flow depth , u and v are depth-averaged velocities in the x and y directions respectively B_x and B_y are the bed topographic elevations while p_1 and p_2 are the volumetric sediment transport rates in the x and y respectively. The equations (3.63) and (3.64) form the complete system of equations governing the sediment transport in two dimensions.

3.1.12 Non-dimensionalization

The non-dimensionalization process is important because the results obtained for a surface experiencing one set of conditions can be applied to a geometrically similar surface experiencing entirely different conditions. Conditions may vary with the nature of fluid, the fluid velocity or the size of the surface. The process also normalizes the boundary layer equations and makes the solution bounded.

In this study the non-dimensionalization will be based on the following sets of scaling variables.$x = x^*L, y = y^*L, t = t^*T, h = h^*L, B = B^*L, g = \frac{L}{T^2}g^*, v = \frac{L}{T}v^*, u = \frac{L}{T}u^*$ where $L = max_{i,j}\left(|x_{i,j} - x_{0,j}, y_{i,j} - y_{i,0}|\right)$ and $T = \sqrt{\frac{L}{g}}$

Writing the first equation of (3.63) in in non-dimensional form, we get;

$$\begin{aligned}
\frac{L}{T}\frac{\partial h^*}{\partial t^*} + \frac{L}{T}\frac{\partial h^*u^*}{\partial x^*} \quad + \quad \frac{L}{T}\frac{\partial h^*v^*}{\partial y^*} &= \frac{E'}{1-\phi} \\
\frac{\partial h^*}{\partial t^*} + \frac{\partial h^*u^*}{\partial x^*} \quad + \quad \frac{\partial h^*v^*}{\partial y^*} &= \frac{T}{L}\frac{E'}{1-\phi} \\
\frac{\partial h^*}{\partial t^*} + \frac{\partial h^*u^*}{\partial x^*} \quad + \quad \frac{\partial h^*v^*}{\partial y^*} &= \frac{1}{\sqrt{gL}}\frac{E'}{1-\phi}
\end{aligned} \tag{3.65}$$

Writing the second equation of (3.63) in a non-dimensional form, we get;

$$\begin{aligned}
\frac{L^2}{T^2}\frac{\partial h^*u^*}{\partial t^*} + \frac{1}{L}\frac{\partial}{\partial x^*}\left(\frac{L^3}{T^2}h^*u^{*2} + \frac{L^3}{2T^2}g^*h^{*2}\right) \quad + \quad \frac{1}{L}\frac{\partial}{\partial y^*}\left(\frac{L^3}{T^2}h^*u^*v^*\right) \\
= \frac{-L^3}{LT^2}\frac{\partial B^*}{\partial x^*} - \frac{L^2}{T^2}g^*h^*s_{fx} \\
\frac{L^2}{T^2}\frac{\partial h^*u^*}{\partial t^*} + \frac{L^2}{T^2}\frac{\partial}{\partial x^*}\left(h^*u^{*2} + \frac{1}{2}g^*h^{*2}\right) \quad + \quad \frac{L^2}{T^2}\frac{\partial}{\partial y^*}\left(h^*u^*v^*\right) \\
= \frac{L^2}{T^2}\left(\frac{\partial B^*}{\partial x^*} - g^*h^*s_{fx}\right) \\
\frac{\partial h^*u^*}{\partial t^*} + \frac{\partial}{\partial x^*}\left(h^*u^{*2} + \frac{1}{2}g^*h^{*2}\right) \quad + \quad \frac{\partial}{\partial y^*}\left(h^*u^*v^*\right) \\
= \left(\frac{\partial B^*}{\partial x^*} - g^*h^*s_{fx}\right)
\end{aligned} \tag{3.66}$$

Writing the third equation of (3.63) in non-dimensional form, we get;

$$\begin{aligned}
\frac{L^2}{T^2}\frac{\partial h^* v^*}{\partial t^*} + \frac{1}{L}\frac{\partial}{\partial x^*}\left(\frac{L^3}{T^2}h^* u^* v^*\right) \quad &+ \quad \frac{1}{L}\frac{\partial}{\partial y^*}\left(\frac{L^3}{T^2}h^* v^{*2} + \frac{L^3}{2T^2}g^* h^{*2}\right) \\
= \frac{-L^3}{LT^2}\frac{\partial B^*}{\partial y^*} - \frac{L^2}{T^2}g^* h^* s_{fy} & \\
\frac{L^2}{T^2}\frac{\partial h^* v^*}{\partial t^*} + \frac{L^2}{T^2}\frac{\partial}{\partial x^*}\left(h^* u^* v^*\right) \quad &+ \quad \frac{L^2}{T^2}\frac{\partial}{\partial y^*}\left(h^* v^{*2} + \frac{1}{2}g^* h^{*2}\right) \\
= \frac{L^2}{T^2}\left(\frac{\partial B^*}{\partial y^*} - g^* h^* s_{fy}\right) & \\
\frac{\partial h^* v^*}{\partial t^*} + \frac{\partial}{\partial x^*}\left(h^* u^* v^*\right) \quad &+ \quad \frac{\partial}{\partial y^*}\left(h^* v^{*2} + \frac{1}{2}g^* h^{*2}\right) \\
= \left(\frac{\partial B^*}{\partial y^*} - g^* h^* s_{fy}\right) &
\end{aligned} \tag{3.67}$$

and finally writing the fourth equation of (3.63) in a non-dimensional form we have;

$$\begin{aligned}
\frac{L}{T}\frac{\partial B^*}{\partial t^*} \quad &+ \quad \xi\frac{T^2}{L}\frac{1}{L}\frac{L^3}{T^3}\frac{\partial p_1^*}{\partial x^*} + \xi\frac{T^2}{L}\frac{1}{L}\frac{L^3}{T^3}\frac{\partial p_2^*}{\partial x^*} = \frac{E'}{1-\phi} \\
\frac{\partial B^*}{\partial t^*} \quad &+ \quad \xi\frac{\partial p_1^*}{\partial x^*} + \xi\frac{\partial p_2^*}{\partial y^*} = \frac{T}{L}\frac{E'}{1-\phi} \\
\frac{\partial B^*}{\partial t^*} \quad &+ \quad \xi\frac{\partial p_1^*}{\partial x^*} + \xi\frac{\partial p_2^*}{\partial y^*} = \frac{1}{\sqrt{gL}}\frac{E'}{1-\phi}
\end{aligned} \tag{3.68}$$

Now dropping the superscripts the set of the specific governing equations in the non-dimensional form are;

$$\begin{aligned} h_t + (hu)_x + (hv)_y &= \frac{E}{1-\phi} \\ (hu)_t + \left(hu^2 + \frac{1}{2}gh^2\right)_x + (huv)_y &= -ghB_x - ghs_{fx} \\ (hv)_t + (huv)_x + \left(hv^2 + \frac{1}{2}gh^2\right)_y &= -ghB_y - ghs_{fy} \\ \frac{\partial}{\partial t}B + \xi\frac{\partial}{\partial x}(p_1) + \xi\frac{\partial}{\partial y}(p_2) &= \frac{E}{1-\phi} \end{aligned} \tag{3.69}$$

where, $E = \beta_0 \left(\frac{\sqrt{u^2+v^2}}{u_c} - 1\right)^{\gamma}$ and $\beta_0 = \frac{\beta}{\sqrt{gL}} = \frac{Fr\beta}{U}$

Chapter 4

NUMERICAL METHODS

In this chapter we write the set of the non-linear hyperbolic conservations laws derived in the previous chapter, using the C formulation. The advantage of writing the conservation laws using this formulation is that it ensures that the Jacobian of the flux matrices F(U) and G(U) i.e. $\frac{\partial F(U)}{\partial U}$ and $\frac{\partial G(U)}{\partial U}$ are non-singular and therefore their respective eigenvalues and their corresponding eigen vectors could be determined. To solve the characteristics equations associated with the Jacobian matrices we use the cubic polynomial formula as given by Spiegiel and Liu (1999). The eigenvalues determined were found to be real and unequal and this demonstrates that the set of system of the nonlinear partial differential equations derived are hyperbolic in nature. These systems of equations admits steady-state solutions in which the non-zero flux terms are balanced by the source terms and also admit solutions that involve discontinuous and non-linear waves, such as shocks and rarefactions as well as wet-dry interfaces generated by dam break flows.

This set of hyperbolic partial differential equations are quite difficult to solve analytically and therefore have to be solved using a suitable numerical method, one which produces low numerical dissipation and diffusion. There are several numerical schemes which can be used to solve these equations such as upwind methods which rely on approximate solutions of non-linear Riemann problems, central schemes also known as Godunov-type schemes on staggered grids, etc.

In this work we shall use a more stable, accurate, simple to use, having comparatively less computer time usage and quite robust schemes called the relaxation schemes. This scheme is based on an approximation on the continuous level before performing the discretizations leading to high-resolution and Riemann solver free methods. The method is also important because it can handle complicated system of conservation laws such as two-phase flow problems like the one in consideration, where we don't expect to have an analytical expression for the physical flux. The main idea behind the relaxation method is to use a local relaxation approximation, by constructing a linear hyperbolic system with a stiff lower order term that approximates the original nonlinear system with a small dissipative correction. The new system can then be solved by under-resolved stable numerical discretizations without using either Riemann solvers spatially or a non-linear system of algebraic equations solver temporally.

Once we have modeled the equations using the C formulation and obtained the eigenvalues, the non-linear hyperbolic equations are converted to a linear hyperbolic system with a relaxation source term which rapidly drives to local

equilibriums in the relaxation limits $\epsilon \rightarrow 0^+$. Introducing the relaxation variables U, V, W a relaxation model is developed to relax the non linear hyperbolic equations. Once the equations have been relaxed we then perform semi-discretization i.e spatial discretization using the Vanleers MUSCL scheme. This scheme is quite powerful and it yields second order accurate in space scheme unlike the upwind stream schemes, see Jin and Xin (1995). Finally we complete the discretization by performing time discretization. To ensure a high order accurate results in time discretization we shall use the fourth order implicit-explicit Runge-Kutta splitting schemes. The splitting treats the source terms implicitly in two steps i.e due to linearity of V and W and then solved explicitly, and the convective terms with two explicit steps. Thus, we have an explicit implementation of implicit source terms, solely determined by the non-stiff convection terms, just as in a usual shock capturing scheme.

At the end of this chapter we specify the initial and the boundary conditions for the dam break scenario having a topography with a narrow deep furrow on downstream location of the breach and a a dam break scenario having topography with two mounds on the downstream location of the breach location.

4.1 C-Formulation

There exists two approaches of rewriting the governing equations in conservation form.

4.1.1 Steady Approach

In the steady approach, the water flow is assumed to be steady and the changes in the bed update have a negligible effect on the water flow, i.e. the wave speed of the bed updating equation is considerably smaller in magnitude than the wave speeds of the water flow. By making these assumptions, the system is decoupled into a water flow approximation, which is iterated to an equilibrium state, followed by a bed update. The steady approach has three formulations namely $A-CV, A-NC, A-SF$ of which the formulation $A-CV$ is the most accurate formulation in the steady approach and is the formulation which is currently in use in the industries. Of the two approaches unsteady approach is the most accurate see, Hudson and Sweby (2003).

4.1.2 Unsteady Approach

In the unsteady approach, no assumptions are made and the water flow and riverbed are calculated simultaneously. With this approach, the water flow can either be steady or unsteady and the changes in the bed update are considered to be significant, i.e. the wave speed of the bed-updating equation is of similar magnitude to the wave speeds of the water flow. For this approach, the system is discretised simultaneously. There are two formulations in the unsteady approach i.e B and C. Formulation C, was found to be more accurate than formulation B and the most accurate of all the formulations in the steady and the unsteady approaches, see Hudson and Sweby (2003).

Therefore to obtain a formulation that is written in a conservative variable form and whose Jacobian matrix is non-singular, we shall adopt the C-formulation

because of it's high level accuracy as compared to other formulations. To obtain the C-formulation we use the product rule to differentiate the source terms of the momentum equations as follows;

$$(ghB)_x = ghB_x + gBh_x \tag{4.1}$$

$$(ghB)_y = ghB_y + gBh_y \tag{4.2}$$

and the momentum equations in the x and y directions takes the form;

$$(hu)_t + (hu^2 + \frac{1}{2}gh^2 + ghB)_x + (huv)_y = -gBh_x - ghs_{fx} \tag{4.3}$$

$$(hv)_t + (huv)_x + (hv^2 + \frac{1}{2}gh^2 + ghB)_y = -gBh_y - ghs_{fy} \tag{4.4}$$

We now get a new system of equations;

$$\begin{aligned} h_t + (hu)_x + (hv)_y &= \frac{E}{1-\phi} \\ (hu)_t + (hu^2 + \frac{1}{2}gh^2 + ghB)_x + (huv)_y &= -gBh_x - ghs_{fx} \\ (hv)_t + (huv)_x + (hv^2 + \frac{1}{2}gh^2 + ghB)_y &= -gBh_y - ghs_{fy} \\ \frac{\partial}{\partial t}B + \xi\frac{\partial}{\partial x}p_1 + \xi\frac{\partial}{\partial y}p_2 &= \frac{E}{1-\phi} \end{aligned} \tag{4.5}$$

The system of equations (4.5) may expressed in a more compact conservative form as follows;

$$U_t + F(U)_x + G(U)_y = S(U) \tag{4.6}$$

Where U is the solution vector defined as;

$$U = \begin{bmatrix} h \\ hu \\ hv \\ B \end{bmatrix}$$

F and G are flux vectors defined as;

$$F(U) = \begin{bmatrix} hu \\ hu^2 + \frac{1}{2}gh^2 + ghB \\ huv \\ \xi p_1 \end{bmatrix}$$

$$G(U) = \begin{bmatrix} hv \\ huv \\ hv^2 + \frac{1}{2}gh^2 + ghB \\ \xi p_2 \end{bmatrix}$$

,

$S(U)$ is the source term defined as;

$$S(U) = \begin{bmatrix} \frac{E}{1-\phi} \\ gBh_x - ghs_{fx} \\ gBh_y - ghs_{fy} \\ \frac{E}{1-\phi} \end{bmatrix}$$

We now obtain the eigen values for the Jacobian of the flux matrices, $\frac{\partial F(U)}{\partial U}$ and $\frac{\partial G(U)}{\partial U}$.

4.2 Eigenvalues for the Jacobian of the flux matrix, F

Now let

$$U = \begin{bmatrix} h \\ hu \\ hv \\ B \end{bmatrix} = \begin{bmatrix} h \\ q_1 \\ q_2 \\ B \end{bmatrix} = \begin{bmatrix} U_1 \\ U_2 \\ U_3 \\ U_4 \end{bmatrix} \tag{4.7}$$

and

$$\begin{aligned} F(U) &= \begin{bmatrix} hu \\ hu^2 + \frac{1}{2}gh^2 + ghB \\ huv \\ Au(u^2+v^2)^{\frac{m-1}{2}} \end{bmatrix} \\ &= \begin{bmatrix} q_1 \\ \frac{q_1^2}{h} + \frac{1}{2}gh^2 + ghB \\ \frac{q_1 q_2}{h} \\ A\xi\left(\frac{q_1^{\frac{2m}{m-1}}}{h^{\frac{2m}{m-1}}} + \frac{q_1^{\frac{2}{m-1}}q_2^2}{h^{\frac{2m}{m-1}}}\right) \end{bmatrix} = \begin{bmatrix} F_1 \\ F_2 \\ F_3 \\ F_4 \end{bmatrix} \end{aligned} \tag{4.8}$$

We now evaluate the Jacobian matrix;

$$\frac{\partial F(U)}{\partial U} = \begin{bmatrix} \frac{\partial F_1}{\partial U_1} & \frac{\partial F_1}{\partial U_2} & \frac{\partial F_1}{\partial U_3} & \frac{\partial F_1}{\partial U_4} \\ \frac{\partial F_2}{\partial U_1} & \frac{\partial F_2}{\partial U_2} & \frac{\partial F_2}{\partial U_3} & \frac{\partial F_2}{\partial U_4} \\ \frac{\partial F_3}{\partial U_1} & \frac{\partial F_3}{\partial U_2} & \frac{\partial F_3}{\partial U_3} & \frac{\partial F_3}{\partial U_4} \\ \frac{\partial F_4}{\partial U_1} & \frac{\partial F_4}{\partial U_2} & \frac{\partial F_4}{\partial U_3} & \frac{\partial F_4}{\partial U_4} \end{bmatrix} =$$

$$\begin{bmatrix} 0 & 1 & 0 & 0 \\ \frac{-(q_1)^2}{h} + gh + gB & \frac{2q_1}{h} & 0 & gh \\ \frac{-q_1 q_2}{h^2} & \frac{q_2}{h} & \frac{q_1}{h} & 0 \\ J_{4,1} & J_{4,2} & J_{4,3} & 0 \end{bmatrix} \tag{4.9}$$

where;

$J_{4,1} = A\xi \frac{2m}{1-m} h^{\frac{3m-1}{1-m}} (q_1^{\frac{2m}{m-1}} + q_1^{\frac{2}{m-1}} q_2^2)$

$J_{4,2} = A\xi h^{\frac{2m}{1-m}} (\frac{2m}{m-1} q_1^{\frac{m+1}{m-1}} + \frac{2}{m-1} (q_1^{\frac{3-m}{m-1}} q_2^2)$

and

$J_{4,3} = 2A\xi h^{\frac{2m}{1-m}} q_1^{\frac{2m}{m-1}} q_2$

We now simplify the Jacobian matrix (4.9) by making the following substitutions;

$$u = \frac{q_1}{h} \tag{4.10}$$

$$v = \frac{q_2}{h} \tag{4.11}$$

$$d = \frac{A\xi}{h^3} \left(3q_1^2 + q_2^2\right) = \frac{A\xi}{h} \left(3u^2 + v^2\right) \tag{4.12}$$

and

$$e = \frac{2A\xi q_1^2 q_2^2}{h^3} = \frac{2A\xi uv}{h} \tag{4.13}$$

simplified matrix becomes;

$$\frac{\partial F(U)}{\partial U} = \begin{bmatrix} 0 & 1 & 0 & 0 \\ g(h+B)-u^2 & 2u & 0 & gh \\ -uv & v & u & 0 \\ -ud-ve & d & e & 0 \end{bmatrix} \tag{4.14}$$

whose characteristic equation is;

$$P(\lambda, W) = \begin{vmatrix} -\lambda & 1 & 0 & 0 \\ g(h+B)-u^2 & 2u-\lambda & 0 & gh \\ -uv & v & u-\lambda & 0 \\ -ud-ve & d & e & -\lambda \end{vmatrix} = 0 \tag{4.15}$$

We expand the above characteristic equation to get;

$$(\lambda - u)\{\lambda^3 - 2u\lambda^2 + [u^2 - g(h+b+hd)]\lambda + ghud\} = 0 \tag{4.16}$$

From this characteristic equation it is quite clear that one of the eigenvalue is;

$$\lambda_1 = u \tag{4.17}$$

To get the other eigenvalues we have to solve the cubic equation;

$$p(\lambda, W) = \{\lambda^3 - 2u\lambda^2 + [u^2 - g(h+b+hd)]\lambda + ghud\} = 0 \tag{4.18}$$

Solving this polynomial analytically is quite involving and difficult and hence we use the formula for the roots of a cubic function as explained in Appendix

A below.

For a cubic equation, the formulae holds only when the roots are real and unequal and therefore we now establish the condition under which our polynomial equation shall be applicable. Using the characteristic equation we find the discriminant as follows;

$$\begin{aligned}\Delta &= \frac{g}{108}\left\{8u^2g\left(h+B\right)^2-u^2\left[4u^2\left(B+h\right)+ghd\left(20\left(h+B\right)+hd\right)\right]\right. \\ &- \left. 4g^2\left(h^3+B^3+h^3d^3+3h\left(d+1\right)\left(h+B\right)\left(hd+B\right)\right)\right\} \qquad (4.19)\end{aligned}$$

and now for all roots to be real and distinct we require that;

$$\begin{aligned}&8u^2g(h+B)^2 < u^2\left[4u^2(B+h)+ghd[20(h+B)+hd)\right] \\ +\ &4g^2\left[h^3+B^3+h^3d^3+3h(d+1)(h+B)(hd+B)\right] \qquad (4.20)\end{aligned}$$

, which is satisfied if the following condition is satisfied;

$$h(x,t)+B(x,t)>0 \qquad (4.21)$$

. But $h(x,t)>0$, hence the condition is satisfied.

Therefore using the formula in Appendix 1 we find that $a_1 = -2u$, $a_2 = u^2 - g(h+B+hd)$, $a_3 = ghud$ which implies that;

$$Q = -\frac{1}{9}\left[u^2+3g\left(h+B+hd\right)\right] \qquad (4.22)$$

and

$$R = -\frac{u}{54}\left[2u^2 - 9g\left(2h + 2B - hd\right)\right] \tag{4.23}$$

and therefore for our polynomial equation the eigenvalues are;

$$\begin{aligned}
\lambda_2 &= = 2\sqrt{-Qcos\left(\frac{1}{3}\theta\right)} - \frac{1}{3}a_1 \\
\lambda_3 &= = 2\sqrt{-Qcos\left(\frac{1}{3}(\theta + 2\pi)\right)} - \frac{1}{3}a_1 \\
\lambda_4 &= = 2\sqrt{-Qcos\left(\frac{1}{3}(\theta + 4\pi)\right)} - \frac{1}{3}a_1
\end{aligned} \tag{4.24}$$

where $cos\theta = \frac{R}{\sqrt{-Q^3}}$.

4.3 Eigenvalues for the Jacobian of the flux Matrix, G

In a similar manner we determine the eigenvalues associated with the flux matrix G;

$$U = \begin{bmatrix} h \\ hu \\ hv \\ B \end{bmatrix} = \begin{bmatrix} h \\ q_1 \\ q_2 \\ B \end{bmatrix} = \begin{bmatrix} U_1 \\ U_2 \\ U_3 \\ U_4 \end{bmatrix} \tag{4.25}$$

and;

$$G(U) = \begin{bmatrix} hv \\ huv \\ hv^2 + \frac{1}{2}gh^2 + ghB \\ Av(u^2+v^2)^{\frac{m-1}{2}} \end{bmatrix} = \begin{bmatrix} q_2 \\ \frac{q_1 q_2}{h} \\ \frac{q_2^2}{h} + \frac{1}{2}gh^2 + ghB \\ A\xi\left(\frac{q_2^{\frac{2m}{m-1}}}{h^{\frac{2m}{m-1}}} + \frac{q_2^{\frac{2}{m-1}}q_1^2}{h^{\frac{2m}{m-1}}}\right) \end{bmatrix} = \begin{bmatrix} G_1 \\ G_2 \\ G_3 \\ G_4 \end{bmatrix} \tag{4.26}$$

We now evaluate the Jacobian matrix;

$$\frac{\partial G(U)}{\partial U} = \begin{bmatrix} \frac{\partial G1}{\partial U_1} & \frac{\partial G_1}{\partial U_2} & \frac{\partial G_1}{\partial U_3} & \frac{\partial G1}{\partial U_4} \\ \frac{\partial G_2}{\partial U_1} & \frac{\partial G_2}{\partial U_2} & \frac{\partial G_2}{\partial U_3} & \frac{\partial G2}{\partial U_4} \\ \frac{\partial G_3}{\partial U_1} & \frac{\partial G_3}{\partial U_2} & \frac{\partial G_3}{\partial U_3} & \frac{\partial G3}{\partial U_4} \\ \frac{\partial G_4}{\partial U_1} & \frac{\partial G_4}{\partial U_2} & \frac{\partial G_4}{\partial U_3} & \frac{\partial G4}{\partial U_4} \end{bmatrix} =$$

$$\begin{bmatrix} 0 & 0 & 1 & 0 \\ \frac{-q_1 q_2}{h} & \frac{q_2}{h} & \frac{q_1}{h} & 0 \\ \frac{-(q_2)^2}{h} + gh + gB & 0 & \frac{2q_2}{h} & gh \\ \tilde{J}_{4,1} & \tilde{J}_{4,2} & \tilde{J}_{4,3} & 0 \end{bmatrix} \tag{4.27}$$

where $\tilde{J}_{4,1} = A\xi\frac{2m}{1-m}h^{\frac{3m-1}{1-m}}(q_1^{\frac{2m}{m-1}} + q_1^{\frac{2}{m-1}}q_2^2)$

$\tilde{J}_{4,2} = A\xi h^{\frac{2m}{1-m}}(\frac{2m}{m-1}q_1^{\frac{m+1}{m-1}} + \frac{2}{m-1}q_1^{\frac{3-m}{m-1}}q_2^2)$

$\tilde{J}_{4,3} = 2A\xi h^{\frac{2m}{1-m}} q_1^{\frac{2m}{m-1}} q_2$

This Jacobian matrix can be simplified by making the following substitutions;

$$u = \frac{q_1}{h} \tag{4.28}$$

$$v = \frac{q_2}{h} \tag{4.29}$$

$$d = \frac{A\xi}{h^3}(3q_1^2 + q_2^2) = \frac{A\xi}{h}(3u^2 + v^2) \tag{4.30}$$

and

$$e = \frac{2A\xi q_1^2 q_2^2}{h^3} = \frac{2A\xi uv}{h} \tag{4.31}$$

The simplified matrix becomes;

$$\frac{\partial G(U)}{\partial U} = \begin{bmatrix} 0 & 0 & 1 & 0 \\ -uv & v & u & 0 \\ g(h+B) - v^2 & 2v & 0 & gh \\ -vd - ue & e & d & 0 \end{bmatrix} \tag{4.32}$$

whose characteristic equation is;

$$P(\beta, W) = \begin{vmatrix} -\beta & 0 & 1 & 0 \\ -uv & v-\beta & u & 0 \\ g(h+B) - v^2 & 0 & 2v-\beta & gh \\ -vd - ue & e & d & -\beta \end{vmatrix} = 0 \tag{4.33}$$

. Expanding the above characteristic equation we get;

$$(\beta - v)\{\beta^3 - 2v\beta^2 + [u^2 - g(h + b + hd)]\beta + ghvd\} = 0 \tag{4.34}$$

From this characteristic equation it is obvious that one of the eigenvalue is;

$$\beta_1 = v \tag{4.35}$$

To get the other eigenvalues we solve the cubic function;

$$p(\beta, W) = \{\beta^3 - 2v\beta^2 + [u^2 - g(h + b + hd)]\beta + ghvd\} = 0 \tag{4.36}$$

Just like for the above polynomial for the characteristic equation of the flux matrix F(U), its quite involving and difficult to say the least, to solve this equation hence we adopt the formulae attached in the Appendix A. Since the formulae holds only when the roots are real and unequal, we shall establish the condition under which this polynomial equation shall be applicable. Using the characteristic equation we find the discriminant as follows;

$$\begin{aligned} \Delta &= \frac{g}{108}\left\{8v^2 g\left(h+B\right)^2 - v^2\left[4v^2\left(B+h\right) + ghd\left(20\left(h+B\right)+hd\right)\right]\right. \\ &- \left. 4g^2\left(h^3 + B^3 + h^3d^3 + 3h\left(d+1\right)\left(h+B\right)\left(hd+B\right)\right)\right\} \end{aligned} \tag{4.37}$$

For all roots to be real and unequal we require that;

$$\begin{aligned} 8v^2 g(h+B)^2 &< v^2\left[4v^2(B+h) + ghd[20(h+B)+hd)\right] \\ &+4g^2\left[h^3 + B^3 + h^3d^3 + 3h(d+1)(h+B)(hd+B)\right] \end{aligned} \tag{4.38}$$

which is satisfied if the following condition is satisfied;

$$h(y,t) + B(y,t) > 0 \tag{4.39}$$

. But $h(y,t) > 0$, hence the condition is satisfied.

Therefore using the formula in appendix A we find that $a_1 = -2v$, $a_2 = v^2 - g(h + B + hd)$, $a_3 = ghvd$ which implies that;

$$Q = -\frac{1}{9}\left[v^2 + 3g\left(h + B + hd\right)\right] \tag{4.40}$$

and

$$R = -\frac{v}{54}\left[2v^2 - 9g\left(2h + 2B - hd\right)\right] \tag{4.41}$$

Therefore we obtain the following eigenvalues;

$$\begin{aligned}
\beta_2 &= 2\sqrt{-Qcos\frac{1}{3}\left(\theta + 2\pi\right)} - \frac{1}{3}a_1 \\
\beta_3 &= 2\sqrt{-Qcos\frac{1}{3}\left(\theta + 2\pi\right)} - \frac{1}{3}a_1 \\
\beta_4 &= 2\sqrt{-Qcos\frac{1}{3}\left(\theta + 4\pi\right)} - \frac{1}{3}a_1
\end{aligned} \tag{4.42}$$

where $cos\theta = \frac{R}{\sqrt{-Q^3}}$.

4.4 Relaxed System of the C-Formulation

To solve the non-linear hyperbolic system (4.5) we shall first convert it to a linear hyperbolic system with a relaxation source term which rapidly drives to a local equilibriums in the relaxation limits $\epsilon \longrightarrow 0^+$. Introducing the artificial variables $\vec{V} = (V_1, V_2, V_3, V_4)$, $\vec{W} = (W_1, W_2, W_3, W_4)$ as the relaxation variables we develop the relaxation model for the system which we write as follows;

$$h_t + v_{1x} + w_{1y} = 0, \tag{4.43}$$

$$q_{1t} + v_{2x} + w_{2y} = 0, \tag{4.44}$$

$$q_{2t} + v_{3x} + w_{3y} = 0, \tag{4.45}$$

$$B_t + v_{4x} + w_{4y} = 0, \tag{4.46}$$

$$v_{1t} + \lambda_1^2 h_x = -\frac{1}{\epsilon}(v_1 - q_1) - \int^x \frac{E}{1-\xi} d\tilde{x}, \tag{4.47}$$

$$v_{2t} + \lambda_2^2 q_{1x} = -\frac{1}{\epsilon}(v_2 - \frac{q_1^2}{h} + \frac{gh^2}{2} + ghB) - \int^x gB\frac{\partial h}{\partial x}(y)d\tilde{x} - Sf_x, \tag{4.48}$$

$$v_{3t} + \lambda_3^2 q_{2y} = -\frac{1}{\epsilon}(v_3 - \frac{q_1 q_2}{h}), \tag{4.49}$$

$$v_{4t} + \lambda_4^2 B_x = -\frac{1}{\epsilon}(v_4 - A\epsilon J_0 - A\epsilon R_0) - \int^x \frac{E}{1-\xi} d\tilde{x}, \tag{4.50}$$

$$w_{1t} + \beta_1^2 h_y = -\frac{1}{\epsilon}(w_1 - q_2), \tag{4.51}$$

$$w_{2t} + \beta_2^2 q_{1x} = -\frac{1}{\epsilon}(w_2 - \frac{q_1 q_2}{h}), \tag{4.52}$$

$$w_{3t} + \beta_3^2 q_{2y} = -\frac{1}{\epsilon}(w_3 - \frac{q_2^2}{h} + \frac{gh^2}{2} + ghB) - \int^y gB\frac{\partial h}{\partial y}(x)d\tilde{y} - Sf_y, \tag{4.53}$$

$$w_{4t} + \beta_4^2 B_x = -\frac{1}{\epsilon}(w_4 - A\epsilon J_0 - A\epsilon R_0). \tag{4.54}$$

where;

$J_0 = \xi\left(\frac{q_1^{\frac{2m}{m-1}}}{h^{\frac{2m}{m-1}}} + \frac{q_1^{\frac{2}{m-1}} q_2^2}{h^{\frac{2m}{m-1}}}\right)$

and

$R_0 = \xi\left(\frac{q_2^{\frac{2m}{m-1}}}{h^{\frac{2m}{m-1}}} + \frac{q_2^{\frac{2}{m-1}} q_1^2}{h^{\frac{2m}{m-1}}}\right)$

Introducing the relaxation variables $\vec{V}, \vec{W}$ to the system (4.6) then the relaxation model above can be written in vector form as follows;

$$\begin{bmatrix} \mathbf{U} \\ \mathbf{V} \\ \mathbf{W} \end{bmatrix} + \begin{bmatrix} 0 & I & 0 \\ \lambda^2 & 0 & 0 \\ 0 & 0 & 0 \end{bmatrix} \begin{bmatrix} \mathbf{U} \\ \mathbf{V} \\ \mathbf{W} \end{bmatrix}_x + \begin{bmatrix} 0 & 0 & I \\ 0 & 0 & 0 \\ \beta^2 & 0 & 0 \end{bmatrix} \begin{bmatrix} \mathbf{U} \\ \mathbf{V} \\ \mathbf{W} \end{bmatrix}_y$$
$$= -\frac{1}{\epsilon} \begin{bmatrix} 0 \\ (V - F(U)) + \tilde{S}(U) \\ (W - G(U)) + \tilde{\tilde{S}}(U) \end{bmatrix} \tag{4.55}$$

where $U = \begin{bmatrix} h \\ q_1 \\ q_2 \end{bmatrix}$, $V = \begin{bmatrix} v_1 \\ v_2 \\ v_3 \end{bmatrix}$, $W = \begin{bmatrix} w_1 \\ w_2 \\ w_3 \end{bmatrix}$,

$$\tilde{S}(U) = \begin{bmatrix} -\int^x \frac{E}{1-\xi} d\tilde{x} \\ -\int^x gB(s,y) \frac{\partial h}{\partial x}(s,y)\, d\tilde{x} \\ 0 \\ \int^x \frac{E}{1-\xi} d\tilde{x} \end{bmatrix} \text{ and } \tilde{\tilde{S}}(U) = \begin{bmatrix} 0 \\ 0 \\ -\int^y gh(x,s) \frac{\partial h}{\partial y}(x,s)\, d\tilde{y} \\ 0 \end{bmatrix}$$

4.5 Spatial Discretization

After relaxing the system we next perform the spatial discretization (semi discretization). Mathematicians have come up with various methods of performing spatial discretization majority of whom use upwind stream. In our case we shall use the Vanleers MUSCL scheme because it has a higher order level of accuracy. Infact it yields a second order accuracy in space scheme unlike the upwind stream which is first order accurate.

We locate the spatial grid points at $(x_{i+\frac{1}{2}}, y_{j+\frac{1}{2}})$ and therefore the grid widths are;

$$\Delta x = x_{i+\frac{1}{2}} - x_{i-\frac{1}{2}} \tag{4.56}$$

in the x direction and;

$$\Delta y = y_{j+\frac{1}{2}} - y_{j-\frac{1}{2}} \tag{4.57}$$

in the y direction;

Let us consider a vector, let say $U = U(x, y)$. We define a point value as

$$U_{(i+\frac{1}{2},j+\frac{1}{2})} = U(x_{i+\frac{1}{2}}, y_{j+\frac{1}{2}}) \tag{4.58}$$

And therefore we define the cell average value as;

$$U_{(i,j)} = \frac{1}{\Delta x \Delta y} \int_{x_{i-\frac{1}{2}}}^{x_{i+\frac{1}{2}}} \int_{y_{i-\frac{1}{2}}}^{y_{i+\frac{1}{2}}} U(x, y) dx dy \tag{4.59}$$

The conservative, semi discrete differencing to (4.55) is;

$$\begin{aligned}
\frac{\partial}{\partial t} U_{i,j} &+ \frac{1}{\Delta x}\left(V_{i+\frac{1}{2},j} - V_{i-\frac{1}{2},j}\right) + \frac{1}{\Delta y}\left(W_{i+\frac{1}{2},j} - W_{i-\frac{1}{2},j}\right) = 0 \\
\frac{\partial}{\partial t} V_{i,j} &+ c^2 \frac{1}{\Delta x}(U_{i+\frac{1}{2},j} - U_{i-\frac{1}{2},j}) = \frac{1}{\epsilon}\left[V_{i,j} - F(U_{i,j}) - \tilde{S}(U_{i,j})\right] \\
\frac{\partial}{\partial t} W_{i,j} &+ d^2 \frac{1}{\Delta y}(U_{i,j+\frac{1}{2}} - U_{i,j-\frac{1}{2}}) = \frac{1}{\epsilon}[W_{i,j} - G(U_{i,j}) - \tilde{\tilde{S}}(U_{i,j})]
\end{aligned} \tag{4.60}$$

where;

c^2= diag $\{\lambda_1^2, \lambda_2^2, \lambda_3^2, \lambda_4^2\}$ and d^2= diag $\{\beta_1^2, \beta_2^2, \beta_3^2, \beta_4^2\}$

The MUSCL piecewise linear interpolation applied to an arbitrary component say, p_{th} component of $v \pm cu$ and $w \pm cu$ gives;

$$\begin{aligned}
(v_p + c_p u_p)_{i+\frac{1}{2},j} &= (v_p + c_p u_p)_{i,j} + \frac{1}{2}\Delta x \sigma^{x,+}_{i,j}, \\
(v_p - c_p u_p)_{i+\frac{1}{2},j} &= (v_p - c_p u_p)_{i+1,j} - \frac{1}{2}\Delta x \sigma^{x,-}_{i+1,j}, \\
(w_p + d_p u_p)_{i,j+\frac{1}{2}} &= (w_p + d_p u_p)_{i,j} + \frac{1}{2}\Delta y \sigma^{y,+}_{i,j}, \\
(w_p - d_p u_p)_{i,j+\frac{1}{2}} &= (w_p - d_p u_p)_{i,j+1} - \frac{1}{2}\Delta y \sigma^{y,-}_{i,j+1},
\end{aligned} \tag{4.61}$$

where u_p, v_p and w_p are the p^{th} components of V, U and W respectively, with σ being the slopes in the $(i,j)th$ cell defined as;

$$\sigma^{x,\pm}_{i,j} = \frac{1}{\Delta x}(v_{p(i+1,j)} \pm c_p u_{p(i+1,j)} - v_{p(i,j)} \mp c_p u_{p(i,j)})\phi(\theta^{x,\mp}_{i,j}) \tag{4.62}$$

with;

$$\theta^{x,\mp}_{i,j} = \frac{v_{p(i,j)} \pm c_p u_{p(i,j)} - v_{p(i-1,j)} \mp c_p u_{p(i-1,j)}}{v_{p(i+1,j)} \pm c_p u_{p(i+1,j)} - v_{p(i,j)} \mp c_p u_{p(i,j)}} \tag{4.63}$$

and;

$$\sigma^{y,\pm}_{i,j} = \frac{1}{\Delta y}(w_{p(i,j+1)} \pm d_p u_{p(i,j+1)} - w_{p(i,j)} \mp d_p u_{p(i,j)})\phi(\theta^{y,\mp}_{i,j}) \tag{4.64}$$

with;

$$\theta^{y,\mp}_{i,j} = \frac{w_{p(i,j)} \pm d_p u_{p(i,j)} - w_{p(i-1,j)} \mp d_p u_{p(i,j-1)}}{w_{p(i,j+1)} \pm d_p u_{p(i,j+1)} - w_{p(i,j)} - d_p u_{p(i,j)}} \tag{4.65}$$

For our scheme (4.61) to be TVD, we impose the following conditions on the limiter function $\phi(\theta)$, Hudson and Sweby (2003), where $\phi(\theta)$ is a sharp slope

limiter called the Vanleer's limiter defined as;

$$\phi(\theta) = \frac{|\theta| + \theta}{1 + |\theta|} \tag{4.66}$$

Following from (4.61) we solve for $u_{i+\frac{1}{2},j}, v_{i+\frac{1}{2},j}$ and $w_{i,j+\frac{1}{2}}$
and get;

$$\begin{aligned} u_{p\left(i+\frac{1}{2},j\right)} &= \frac{1}{2}\left(u_{p(i,j)} + u_{p(i+1,j)}\right) - \frac{1}{2c_p}\left(v_{p(i+1,j)} - v_{p(i,j)}\right) + \frac{\Delta x}{4c_p}\left(\sigma_{i,j}^{x,+} + \sigma_{i+1,j}^{x,-}\right) \\ v_{p\left(i+\frac{1}{2},j\right)} &= \frac{1}{2}(v_{p(i,j)} + v_{p(i+1,j)}) - \frac{c_p}{2}(u_{p(i+1,j)} - u_{p(i,j)}) + \frac{\Delta x}{4}(\sigma_{i,j}^{x,+} - \sigma_{i+1,j}^{x,-}) \end{aligned} \tag{4.67}$$

$$\begin{aligned} u_{p\left(i,j+\frac{1}{2}\right)} &= \frac{1}{2}(u_{p(i,j)} + u_{p(i,j+1)}) - \frac{1}{2d_p}(w_{p(i,j+1)} - w_{p(i,j)}) + \frac{\Delta y}{4d_p}(\sigma_{i,j}^{y,+} + \sigma_{i,j+1}^{y,-}) \\ w_{p\left(i,j+\frac{1}{2}\right)} &= \frac{1}{2}(w_{p(i,j)} + w_{p(i,j+1)}) - \frac{d_p}{2}(u_{p(i,j+1)} - u_{p(i,j)}) + \frac{\Delta y}{4}(\sigma_{i,j}^{y,+} - \sigma_{i,j+1}^{y,-}) \end{aligned} \tag{4.68}$$

substituting (4.67) and (4.68) into (4.60) we obtain;

$$\begin{aligned}
\frac{\partial}{\partial t}u_{p(i,j)} &+ \frac{1}{2\Delta x}(v_{p(i+1,j)} - v_{p(i-1,j)}) - \frac{c_p}{2\Delta x}(u_{p(i+1,j)} - 2u_{p(i,j)} + u_{p(i-1,j)}) \\
&- \frac{d_p}{2\Delta y}(w_{p(i,j+1)} - 2w_{p(i,j)} + w_{p(i,j-1)}) \\
&+ \frac{1}{4}(\sigma_{i,j}^{x,+} - \sigma_{i+1,j}^{x,-} - \sigma_{i-1,j}^{x,+} + \sigma_{i,j}^{x,-} + \sigma_{i,j}^{y,+} + \sigma_{i,j+1}^{y,-} - \sigma_{i,j-1}^{y,+} + \sigma_{i,j}^{y,-}) = 0, \\
\frac{\partial}{\partial t}v_{i,j} &+ \frac{c_p^2}{2\Delta x}(u_{p(i+1,j)} - u_{p(i-1,j)}) - \frac{c_p}{2\Delta x}(v_{p(i+1,j)} - 2v_{p(i,j)} + v_{p(i-1,j)}) \\
&+ \frac{c_p}{4}(\sigma_{i,j}^{x,+} + \sigma_{i+1,j}^{x,-} - \sigma_{i-1,j}^{x,+} + \sigma_{i,j}^{x,-}) = -\frac{1}{\epsilon}(v_{p(i,j)} - F_p(u_{p(i,j)})) - \frac{1}{\epsilon}\tilde{S}_p(u_{i,j}) \\
\frac{\partial}{\partial t}w_{p(i,j)} &+ \frac{d_p^2}{2\Delta y}(u_{p(i,j+1)} - u_{p(i,j-1)}) - \frac{d_p}{2\Delta y}(w_{p(i,j+1)} - 2w_{p(i,j)} + v_{p(i,j-1)}) \\
&+ \frac{d_p}{4}(\sigma_{i,j}^{y,+} + \sigma_{i+1,j}^{y,-}) - \sigma_{i-1,j}^{y,+} + \sigma_{i,j}^{y,-}) = -\frac{1}{\epsilon}(w_{p(i,j)} - G_p(u_{p(i,j)})) - \frac{1}{\epsilon}\tilde{\tilde{S}}_p(u_{p(i,j)})
\end{aligned}$$

where $\tilde{S}_p, \tilde{\tilde{S}}_p, F_p$ and G_p are the p^{th} components of $\tilde{S}, \tilde{\tilde{S}}, F$ and G respectively.

4.6 Time Discretization

In this section we present the time discretization of the semi-discrete relaxation schemes performed in the above section. To carry out this process accurately we shall apply the second-order implicit-explicit Runge-Kutta splitting scheme as the time marching mechanism to advance the solution by one time step Δt. The splitting treats, alternatively the source terms $\frac{1}{\epsilon}(V - F(U) + \tilde{S}(U))$ and $\frac{1}{\epsilon}(W - G(U) + \tilde{\tilde{S}}(U))$ implicitly in two steps i.e. due to the linearity of v and w which shall then be solved explicitly, and the convection terms with two explicit steps. The resulting scheme shall be linear;

Let $\Delta t = t^{n+1} - t^n$. Since U^n, V^n and W^n are known values we compute the

values for U^{n+1}, V^{n+1} and W^{n+1} as follows;

$$
\begin{aligned}
u_p^{n,1} &= u_p^n, \\
v_p^{n,1} &= v_p^n + \tfrac{\Delta t}{\epsilon}(v_p^{n,1} - F(u_p^{(n,1)}) + \tfrac{\Delta t}{\epsilon}\tilde{S}(u_p^{n,1}), \\
w_p^{n,1} &= w_p^n + \tfrac{\Delta t}{\epsilon}(w_p^{n,1} - G(u_p^{n,1}) + \tfrac{\Delta t}{\epsilon}\tilde{\tilde{S}}(u_p^{n,1}); \\
u_p^1 &= u_p^{n,1} - \Delta t(\Delta_+^x v_p^{n,1} + \Delta_+^y w_p^{n,1}), \\
v_p^1 &= v_p^{n,1} - \Delta t c^2 \Delta_+^x u_p^{n,1}, \\
w_p^1 &= w_p^{n,1} - \Delta t d^2 \Delta_+^y u_p^{n,1}, \\
u_p^{n,2} &= u_p^1, \\
v_p^{n,2} &= v_p^1 - \tfrac{\Delta t}{\epsilon}(v_p^{n,2} - F(u_p^{(n,2)}) - \tfrac{2\Delta t}{\epsilon}(v_p^{n,1} - F(u_p^{(n,1)}) \quad - \quad \tfrac{\delta t}{\epsilon}\tilde{S}u_p^{(n,2)} - \tfrac{2\Delta t}{\epsilon}\tilde{S}(u_p^{n,1}), \\
w_p^{n,2} &= w_p^1 - \tfrac{\Delta t}{\epsilon}(w_p^{n,2} - G(u_p^{(n,2)}) - \tfrac{2\Delta t}{\epsilon}(v_p^{n,1} - F(u_p^{(n,1)}) \quad - \quad \tfrac{\delta t}{\epsilon}\tilde{S}(u_p^{n,2}) - \tfrac{2\Delta t}{\epsilon}\tilde{S}(u_p^{n,1}) \\
u_p^{(2)} &= u_p^{n,2} - \Delta t(\Delta_+^x v_p^{n,2} + \Delta_+^y w_p^{n,2}), \\
v_p^{(2)} &= v_p^{n,2} - \Delta t c^2 \Delta_+^x u_p^{n,2}, \\
w_p^{(2)} &= w_p^{n,2} - \Delta t d^2 \Delta_+^y u_p^{n,2}, \\
u_p^{n+1} &= \tfrac{1}{2}(u_p^n + u_p^2), \\
v_p^{n+1} &= \tfrac{1}{2}(v_p^n + v_p^2), \\
w_p^{n+1} &= \tfrac{1}{2}(w_p^n + w_p^2),
\end{aligned}
\tag{4.69}
$$

This relaxation scheme has been made stable under the CFL condition $Max\left((max\,(c_i))\,\frac{\Delta t}{\Delta x}, (max\,(d_i))\,\frac{\Delta t}{\Delta y}\right)$ The terms in $\tilde{S}$ and $\tilde{\tilde{S}}$ in the numerical scheme was evaluated using the trapezoidal rule as follows;

$h\,(x,y) \equiv h\,(x_i, y_i) = h_{i,j}$

$$B(x,y) \equiv B(x_i, y_i) = B_{i,j}$$

$$-\int^{x} gh(s,y)\frac{\partial B}{\partial x}(s,y)\,ds \approx \frac{g}{4}\left[h_{i,j}\left(B_{i+1,j}-B_{i-1,j}\right)+h_{i+1,j}\left(B_{i+2,j}-B_{i,j}\right)\right] \tag{4.70}$$

$$-\int^{x} gh(x,s)\frac{\partial B}{\partial y}(x,s)\,ds \approx \frac{g}{4}\left[h_{i,j}\left(B_{i,j+1}-B_{i,j-1}\right)+h_{i,j+1}\left(B_{i,j+2}-B_{i,j}\right)\right] \tag{4.71}$$

$$\pm\int^{x} \frac{E(s,y)}{1-\phi}ds \approx \frac{\pm 1}{2(1-\phi)}\left[E_{i+1,j}+E_{i,j}\right] \tag{4.72}$$

4.7 The initial and boundary conditions

4.7.1 Specification of the initial conditions

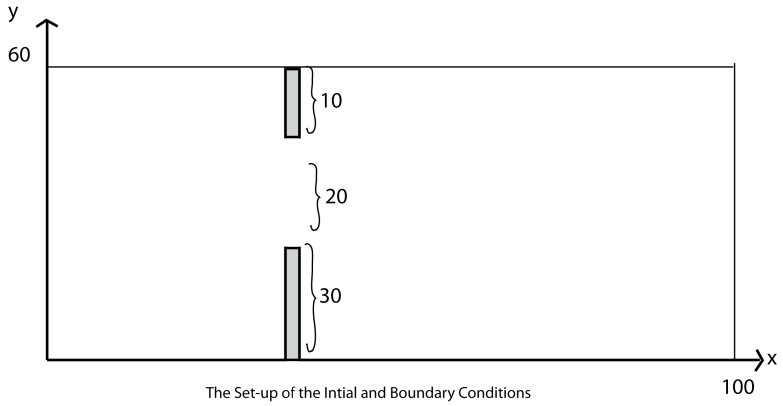

Figure 4.1: The set-up of the initial and Boundary Conditions

We specify the initial conditions for the dam break scenario using the following Riemann data;

$$U^{L,R}(x,y,0) \equiv U^{L,R} = \left[u_1^{L,R}, u_2^{L,R}, u_3^{L,R}, u_4^{L,R}\right]^T \tag{4.73}$$

The topography $u_4^{L,R}$ is specified as below:

1. In the case of a furrow;

$$u_1^L = 6, u_2^L = 0, u_3^L = 0$$
$$u_1^R = 2, u_2^R = 0, u_3^R = 0 \tag{4.74}$$

$$u_4^{L,R} = B(x, y, 0) \equiv 2 - 2X(x)\, Y(y) \tag{4.75}$$

where $Y(y)$ is specified using the Gaussian distribution function;

$$normpdf(y, \mu, \sigma) = normpdf(y, 40, 3) \tag{4.76}$$

and $X(x)$ is specified using the hyperbolic function;

$$\tilde{X}(x) = 2tanh(15 - 0.27x) \tag{4.77}$$

$$X(x) = max\left(\tilde{X}(x)\right) - \tilde{X}(x) \tag{4.78}$$

2. In the case of the two mounds;

$$u_1^L = 1, u_2^L = 0, u_3^L = 0$$
$$u_1^R = 0, u_2^R = 0, u_3^R = 0 \tag{4.79}$$

$$u_4^{L,R} = B(x, y, 0) \equiv 60X_1(x)\, Y_1(y) + 75X_2(x)\, Y_2(y) \tag{4.80}$$

where;

$$\begin{aligned} X_1(x) &= normpdf\,(x, 70, 4) \\ Y_1(y) &= normpdf\,(y, 20, 4) \\ X_2(x) &= normpdf\,(x, 70, 4) \\ Y_2(y) &= normpdf\,(y, 40, 4) \end{aligned} \tag{4.81}$$

The initial conditions for vectors V and W are written using vector U as follows;

$$V^{L,R} = F\left(U^{L,R}\right) \tag{4.82}$$

and;

$$W^{L,R} = G\left(U^{L,R}\right) \tag{4.83}$$

4.7.2 Specification of the Boundary Conditions

The boundary conditions at the breach position are assumed to be transmissive and all other boundaries are considered reflective. We use two ghost cells at the end points of the interval of x and y i.e. x_1, x_2 and x_{N-1}, x_N for $x_1 \leq x \leq x_N$ and y_1, y_2 and y_{N-1}, y_N for $y_1 \leq y \leq y_N$.

Notice that $x_1 = y_1 = 0, x_N = 100, Y_N = 60$ with the number of subdivisions taken as 60. Therefore using these ghost cells we define the boundary conditions

on $x-$ axis and $y-$ axis respectively as below:

$$\begin{aligned}
U(x_1 : x_2, y, t) &= U(0 : 1, y, t) \equiv U(2, y, t)\, for 0 \leq y \leq 60, t \geq 0, \\
U(x_{N-1} : x_N, y, t) &= U(99 : 100, y, t) \equiv U(98, y, t)\, for 0 \leq y \leq 60, t \geq 0, \\
V(x_1 : x_2, y, t) &= V(0 : 1, y, t) \equiv V(2, y, t)\, for 0 \leq y \leq 60, t \geq 0, \\
V(x_{N-1} : x_N, y, t) &= V(99 : 100, y, t) \equiv V(98, y, t)\, for 0 \leq y \leq 60, t \geq 0, \\
W(x_1 : x_2, y, t) &= W(0 : 1, y, t) \equiv W(2, y, t)\, for 0 \leq y \leq 60, t \geq 0, \\
W(x_{N-1} : x_N, y, t) &= W(99 : 100, y, t) \equiv W(98, y, t)\, for 0 \leq y \leq 60, t \geq 0,
\end{aligned} \tag{4.84}$$

$$\begin{aligned}
U(x, y_1 : y_2, t) &= U(x, 0 : 1, t) \equiv U(x, 2, t)\, for 0 \leq x \leq 100, t \geq 0, \\
U(x, y_{N-1} : y_N, t) &= U(x, 59 : 60, t) \equiv U(x, 58, t)\, for 0 \leq x \leq 100, t \geq 0, \\
V(x, y_1 : y_2, t) &= V(x, 0 : 1, t) \equiv V(x, 2, t)\, for 0 \leq x \leq 100, t \geq 0, \\
V(x, y_{N-1} : y_N, t) &= V(x, 59 : 60, t) \equiv V(x, 58, t)\, for 0 \leq x \leq 100, t \geq 0, \\
W(x, y_1 : y_2, t) &= W(x, 0 : 1, t) \equiv W(x, 2, t)\, for 0 \leq x \leq 100, t \geq 0, \\
W(x, y_{N-1} : y_N, t) &= W(x, 59 : 60, t) \equiv W(x, 58, t)\, for 0 \leq x \leq 100, t \geq 0,
\end{aligned} \tag{4.85}$$

4.7.3 Specification of the flow variables at the wall in the case of the furrow

Let the wall be located at X_{50} (i.e. the index where $x = 50$), then the conditions at the wall for $y \leq 30$ and $y \geq 50$ are given by:

Upstream of the wall

$$
\begin{aligned}
U\left(49:50,0:30,t\right) &\equiv U\left(2,0:30,t\right) t \geq 0 \\
U\left(49:50,50:60,t\right) &\equiv U\left(2,50:60,t\right) t \geq 0 \\
V\left(49:50,0:30,t\right) &\equiv V\left(2,0:30,t\right) t \geq 0 \\
V\left(49:50,50:60,t\right) &\equiv V\left(2,50:60,t\right) t \geq 0 \\
W\left(49:50,0:30,t\right) &\equiv W\left(2,0:30,t\right) t \geq 0 \\
W\left(49:50,50:60,t\right) &\equiv W\left(2,50:60,t\right) t \geq 0
\end{aligned}
\tag{4.86}
$$

Downstream of the wall

$$
\begin{aligned}
U\left(51:52,0:30,t\right) &\equiv U\left(98,0:30,t\right) t \geq 0 \\
U\left(51:52,50:60,t\right) &\equiv U\left(98,50:60,t\right) t \geq 0 \\
V\left(51:52,0:30,t\right) &\equiv V\left(98,0:30,t\right) t \geq 0 \\
V\left(51:52,50:60,t\right) &\equiv V\left(98,50:60,t\right) t \geq 0 \\
W\left(51:52,0:30,t\right) &\equiv W\left(98,0:30,t\right) t \geq 0 \\
W\left(51:52,50:60,t\right) &\equiv W\left(98,50:60,t\right) t \geq 0
\end{aligned}
\tag{4.87}
$$

4.7.4 Specification of the flow variables at the wall in the case of the mounds

Let the wall be located at x_{50} (i.e. the index where $x = 50$). Then the conditions at the wall for $y \leq 20$ and $y \geq 50$ are given by:

Upstream of the wall

$$\begin{aligned} U(49:50, 0:20, t) &\equiv U(2, 0:20, t)\, t \geq 0 \\ U(49:50, 50:60, t) &\equiv U(2, 50:60, t)\, t \geq 0 \\ V(49:50, 0:20, t) &\equiv V(2, 0:20, t)\, t \geq 0 \\ V(49:50, 50:60, t) &\equiv V(2, 50:60, t)\, t \geq 0 \\ W(49:50, 0:20, t) &\equiv W(2, 0:20, t)\, t \geq 0 \\ W(49:50, 50:60, t) &\equiv W(2, 50:60, t)\, t \geq 0 \end{aligned} \tag{4.88}$$

Downstream of the wall

$$\begin{aligned} U(51:52, 0:20, t) &\equiv U(98, 0:20, t)\, t \geq 0 \\ U(51:52, 50:60, t) &\equiv U(98, 50:60, t)\, t \geq 0 \\ V(51:52, 0:20, t) &\equiv V(98, 0:20, t)\, t \geq 0 \\ V(51:52, 50:60, t) &\equiv V(98, 50:60, t)\, t \geq 0 \\ W(51:52, 0:20, t) &\equiv W(98, 0:20, t)\, t \geq 0 \\ W(51:52, 50:60, t) &\equiv W(98, 50:60, t)\, t \geq 0 \end{aligned} \tag{4.89}$$

Based on the fully discretized scheme (4.69), the initial conditions (4.74), (4.75), (4.79) and (4.80) and the boundary conditions (4.84), (4.85), (4.86), (4.87), (4.88) and (4.89) a computer code was developed using the Matlab programming language to simulate the results.

The model applicability was examined by simulating the scenarios of a dam break flows in the two topographic surfaces viz: a topographic surface with a furrow and a topographic surface with two mounds located in the downstream of the breach location. In the next chapter we discuss the results thus obtained.

Chapter 5

RESULTS AND DISCUSSION

This chapter is divided in three sections. Section one presents the results of the bed load transport and morphological evolution of a topography containing a narrow deep furrow located downstream of the breach location on dam break scenarios with entrainment and without entrainment. Section two presents the results of the bed load transport and morphological evolution of a topography having two mounds located downstream of the breach location on dam break scenarios with entrainment and without entrainment. While section three presents the conclusion of study and the recommendations for further research.

5.1 Morphological evolution of a furrow located downstream of the dam breach.

In this section we present results on the effect of the entrainment and morphological evolution of a topography containing a narrow deep furrow located on the downstream of the breach location after a sudden dam breach.

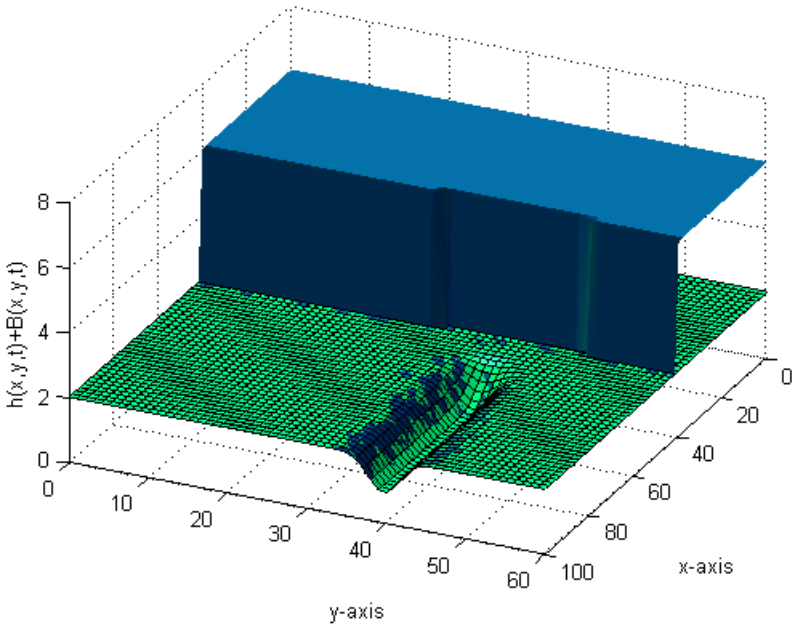

Figure 5.1: The Initial Set-up of the topography and the dam shortly before the dam break.

The figure 5.1 shows the initial set-up of the dam before the dam break, the topography is as defined by (4.75). The water depth upstream of the dam was set to a non-dimensional value of 6 with a downstream depth set at a non-dimensional value of 2 creating a bore wave which propagates downstream whilst a depression wave travels upstream, both spreading laterally as can be seen in figures 5.4 and 5.5. The computation domain is 100×60 which has been subdivided into rectangular grids of dimensions $\Delta x = 1.67$ and $\Delta y = 1$. The CFL condition was set as 0.8, the Froudes number as 0.5 while the constant A in the Grass formula (3.56) and (3.57) was set as 0.001. The frictional force was set to a value of $f = 0.0018$, where f is the Darcy Weisbach factor. The breach is 20 units wide as shown in the figure 4.1

Figure 5.2: Glashutte Embankment dam overtopping on 12th August 2002 shortly before dam failure.
Source:http:espace.uq.edu.au/eserv/UQ:18350/chanson nova09.pdf

The figure 5.2 is a photograph capturing a scenario of a dam just a short time before a dam break which occurred in Glashutte, Germany. Since this is a real life case of occurrence it validates our scenario of a possible dam break which would occur unexpectedly and even cause a catastrophic damage. The figure 5.1 in our simulations is synonymous to the figure 5.2 in the real life situation.

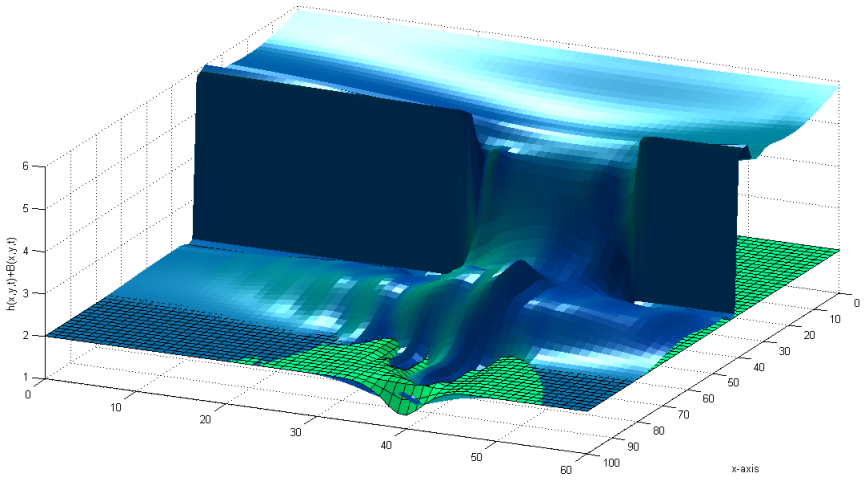

Figure 5.3: Water depth rise after the partial dam break.

The figure 5.3 shows the scenario after the dam break. This figure shows the water waves as it exits from breach and advance in the downstream topography causing the flooding. The figure 5.4 shows the velocity vector plots and the

water depth contours on the considered topography after the dam break. The key attached to the figure 5.4 shows the water height distributions on the dam breach and some distance away from the dam breach, in both upstream and downstream locations. The flood depths distributions are measures of the flood inundations.

The figure 5.5 is the zoom of the figure 5.4 and it shows the flood depths distribution of the water waves from point $x = 55$ to $x = 100$. These figures shows the development of the bore at the time period $T = 2$ which is half the total period. These results are validated by those obtained in the literature see Fennema and Chaudhry (1990). From these results its clear that the water depth downstream is highest near the breach and decreases as water waves progresses further downstream along the furrow.

The figure 5.6 shows a real life scenario of entrainment due to a failure of the 207 feet high Auburn Cofferdam in America on February 18, 1986, when 100,000 cubic feet per second was pouring downstream. The photograph is meant to validate our simulations (Figure 5.5), on how flooding downstream cause erosion, transport debris which are then deposited at various locations. The figure 5.7 shows the velocity vector contours of the flow. The attached key shows the magnitudes of the velocities of the flow field as it progresses downstream from the breach location. The velocity is highest near the breach and decreases as it progresses down the furrow. This is because of the fact that as water moves along the furrow there is scouring effects, the sides of the furrow

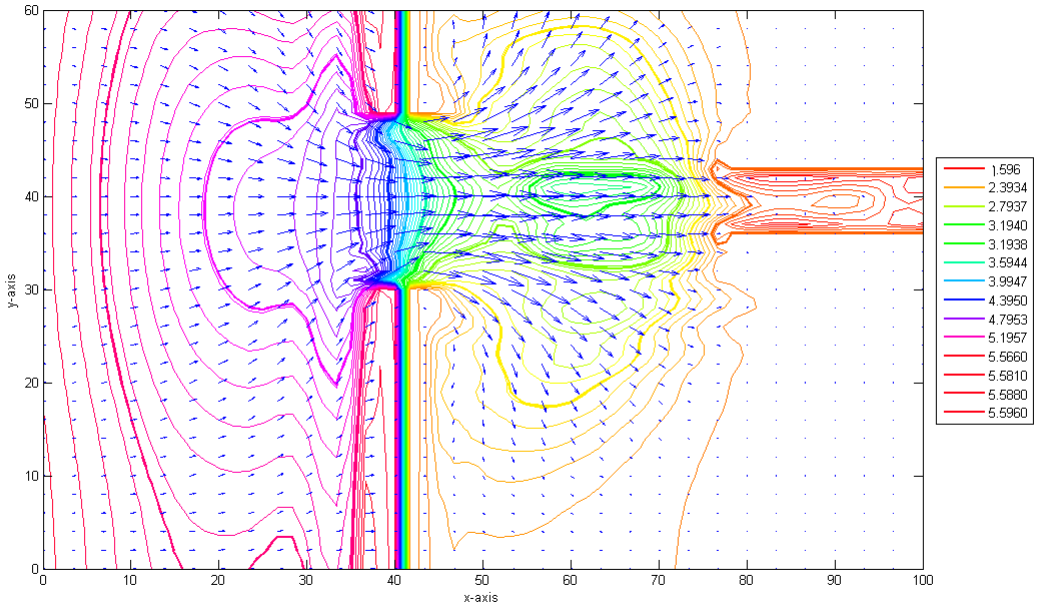

Figure 5.4: The Depth contours and velocity vector plots for the partial dam -break flow.

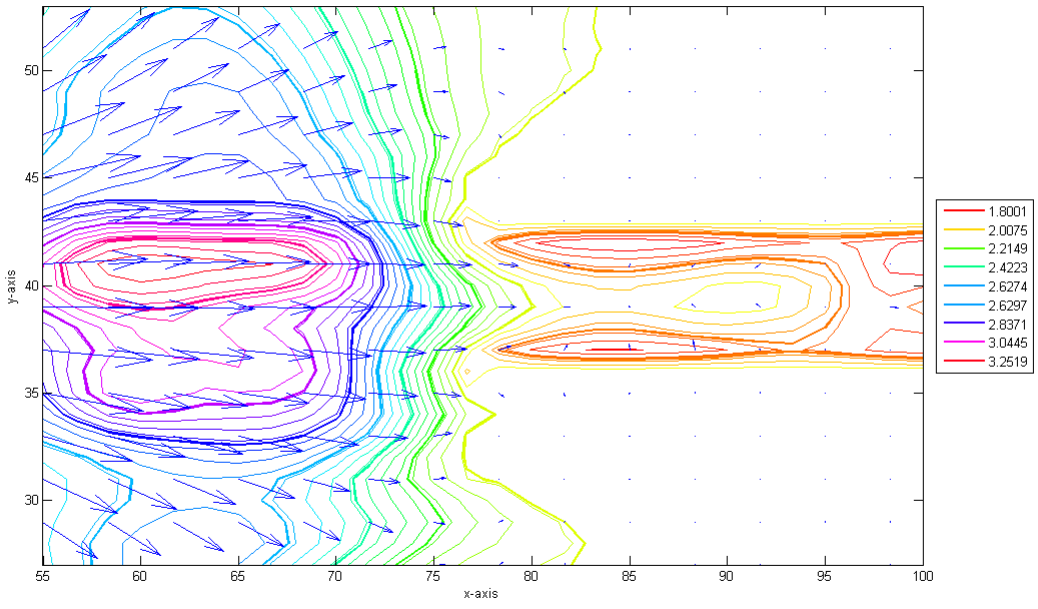

Figure 5.5: The Depth contours and velocity vector plots for the partial dam -break flow zoomed to show the progress of entrainment from $x = 55$ to $x = 100$.

Figure 5.6: Failure of the 207 feet high Auburn Cofferdam on the American river on February 18 1986.

are eroded and transported along the furrow as bed load with a relatively lower velocity.

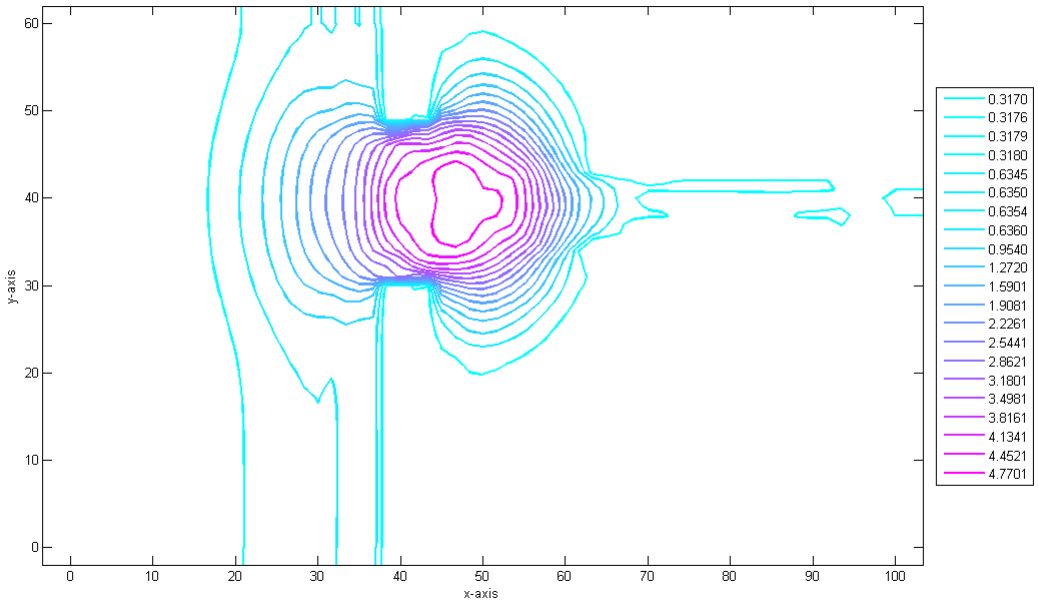

Figure 5.7: The velocity vector contours and their corresponding magnitudes.

The figure 5.8 and the figure 5.9 compares two scenarios of the morphological change of the furrow both at computation time $T = 2$, i.e. at half the computation time with and without the entrainment respectively. From the two

figures its clear that the presence of the entrainment factor leads to a greater morphological change of the furrow than without the entrainment factor. This because of the fact there is more shearing force and greater bed load deposition in the downstream flow with the entrainment than the downstream flow without the entrainment factor.

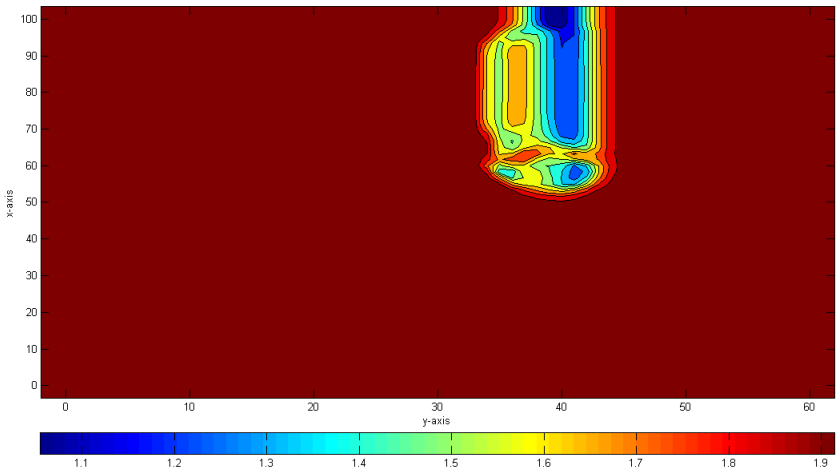

Figure 5.8: Aerial view of the furrow at T=2 for a dam break scenario without the entrainment.

The figure 5.10 compares the aerial views of the furrow before and after the erosion process as a result of the dam break and with entrainment into play. The figure on the right is a representation of the morphological change which the topography has undergone. The furrow is wider and shallower as compared to the original furrow. The widening of the furrow is possibly due to the scouring effects of the sides of the furrow due to the entrainment while the deposition of the eroded sediments at the furrow bottom make it shallower.

The figure 5.11 shows the furrow profiles taken at three different time intervals i.e. at $T = 1.5, T = 3$ and $T = 4$. The three profiles are distinctly

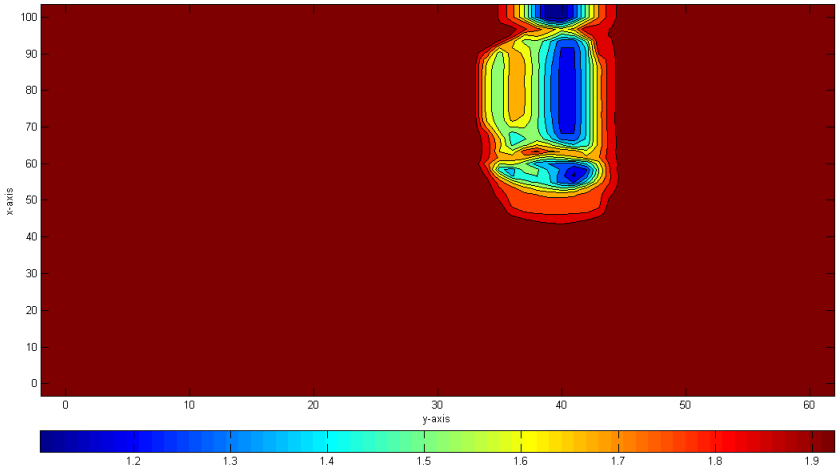

Figure 5.9: Aerial view of the furrow at the period T=2 for the dam break scenario with entrainment.

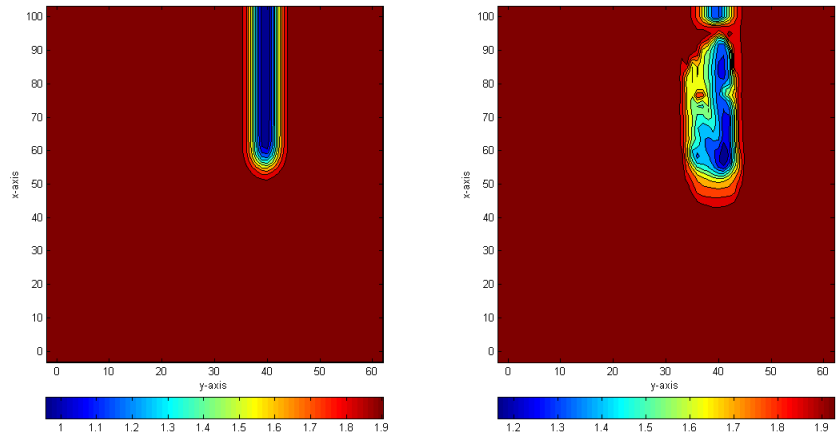

Figure 5.10: Aerial views of the topography before the dam break and after the dam break for the dam break scenario with the entrainment.

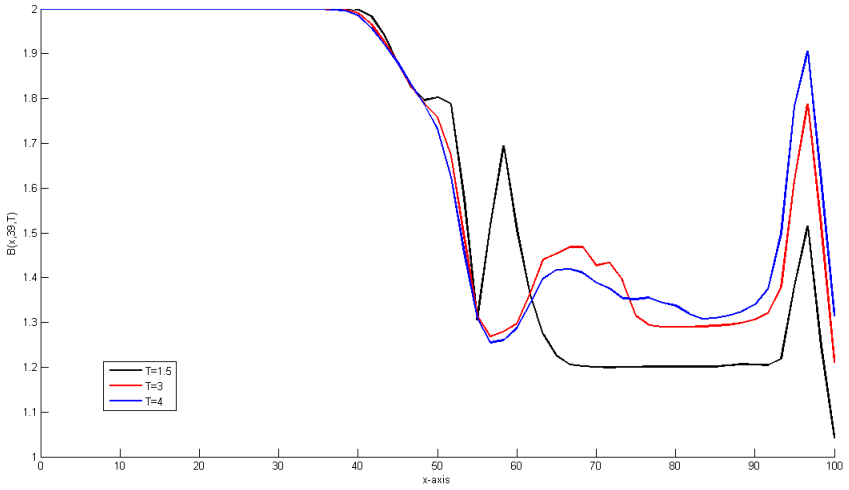

Figure 5.11: Aerial view of the furrow at periods T=1.5, T=3 and T=4 for a dam break scenario with the entrainment.

represented by the black, red and blue colored hydro-graphs respectively. As the entrainment process continues the transported sediments which has been eroded from the furrow is deposited at the bottom. This is shown in the three hydro-graphs between the distances $x = 50$ and $x = 80$. The rest of the sediments is deposited at the furrow end at the distance $x = 95$ as shown in the graph. The deposition at $x = 55$ is due to bed eroded in the first impact of the dam break while the deposition at $x = 95$ is the load deposited in the course of the entrainment flow. This is consistent with the bed-load mass conservation equation 4.5.

The figure 5.12 compares the the furrow profiles with and without the entrainment. The blue profile represent the furrow profile without the entrainment while the red profile represent the furrow profile with the entrainment taken into account. From the results it can be observed that the morphological evolution is more pronounced in the presence of the entrainment

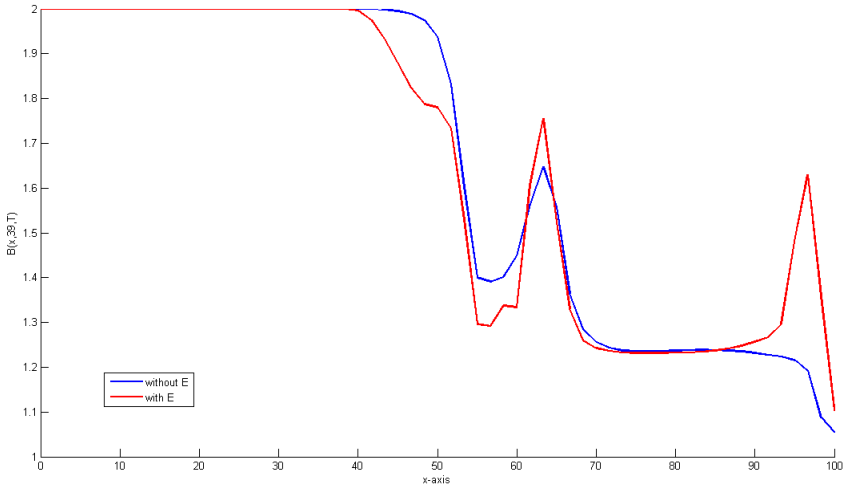

Figure 5.12: The comparison of the furrow profiles in the dam break scenario with entrainment and without the entrainment.

than without the entrainment. Comparing the graphs in the region $x = 40$ to 50 and $x = 50$ to 60, it's observed that for the dam break scenario with the entrainment there is more scouring effects of the furrow than in the dam break scenario without the entrainment. Similarly with the dam break scenario with entrainment, there is more deposition of the load than in the dam break scenario without the entrainment, see regions $x = 60$ to 70 and $x = 90$ to 100.

5.2 Morphological evolution of two mounds located downstream of the dam breach

In this section we present the results of the morphological evolution of the topography with two mounds located in the downstream of the breach location on a dam break scenario with entrainment and on a dam break scenario without the entrainment. The mounds represents obstacles which can be found within the vicinity of the dam break such as infrastructures, buildings or homes. After the violent impact of the water waves on the mounds, the flow is forced to change its direction to pass the mounds, but finally encircles the mounds. Then further downstream the flow slowly recovers the structure it would have without obstruction.

The considered topography is as defined by the equation (4.79), the computation domain is 100×60 and the breach is 30 units wide. At the instant of dam break the water upstream of the breach starts to pour downstream and propagates in form of water waves which moves in the positive direction (taken to be the direction of the water flow) and comes into impact with the obstacles, in the considered topography i.e. the mounds located in the direction of the wave. On impact, the water waves interacts with the mounds at an angle and are reflected off the mounds at the same corresponding angle, undergoing Clapotis gaufre motion see Richardson *et al.* (2002). As a result there is interaction of the water waves leading to a drastic reduction in speed. The flood depth on this part of the region increases from zero covering the mounds partially as shown in figures 5.13 and 5.14. This scenario in real life

situation would cause flooding which is harzadous to human and animal lives as shown in the figure 5.15. The results are validated by other results found for this problem in the literature see Mingham and Causon (1998) who used the Godunov type method to model a problem of simultaneous breach of a dam in a frictionless horizontal channel.

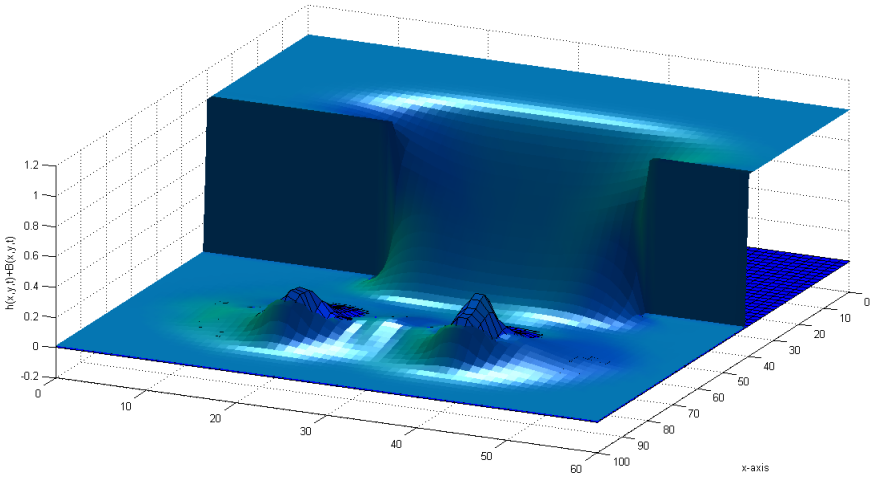

Figure 5.13: Dam break flow scenario with entrainment.

The figure 5.13 shows the dam break scenario with entrainment on a topographic surface containing two mounds located on the downstream of the breach location while the figure 5.14 is a dam break scenario without the entrainment on a topographic surface with two mounds located downstream of the breach location. From the results it's observed that the water heights are higher in a scenario of dam break with entrainment than without the entrainment. This observation is well interpreted by the flood depths magnitudes in the figures 5.16 and 5.17. The higher water heights is due to the greater deposition of the eroded beds causing more possible blockage and reduced entrainment flow.

The figure 5.15 is a photograph showing flooding in Glashutte, Germany after a dam break. The scenario is captured to show a real life situation of a flood inundation, the mounds in this case are represented by the buildings which have been submerged in the flood. This event is therefore a validation of the dam break scenario represented by the figures 5.14 and 5.13. The event is a

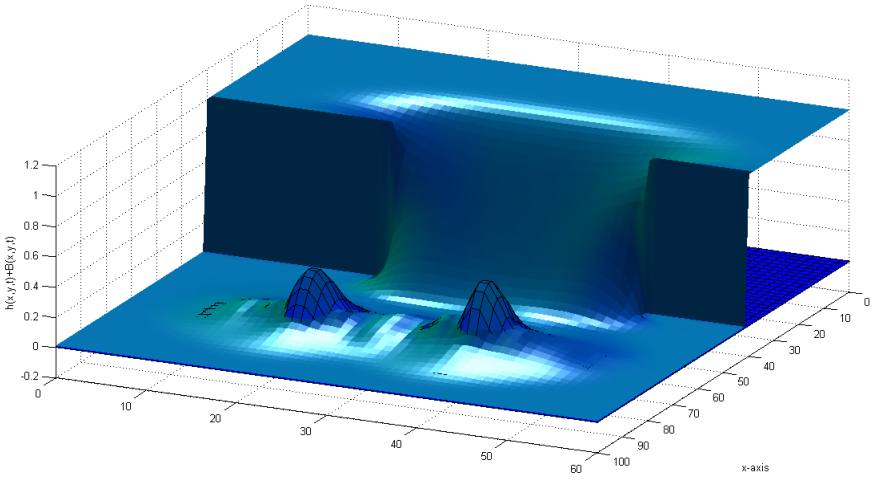

Figure 5.14: Dambreak scenario without the entrainment.

proof that in the case of failure of proper flood protection measures, the damage potential resulting from a dam break is often very high.

Figure 5.15: The Flooding in Glashutte after the dam break.
Source:http:espace.uq.edu.au/eserv/UQ:18350/chanson nova09.pdf.

Figures 5.16 and 5.17 shows the velocity vector plots and the water depth contours after the partial dam break. From the figures it can be observed that flood inundation is more intense in the case of a dam break scenario with entrainment than without the entrainment. However, in both cases the flood

depth decreases as the water waves progresses downstream from the breach location.

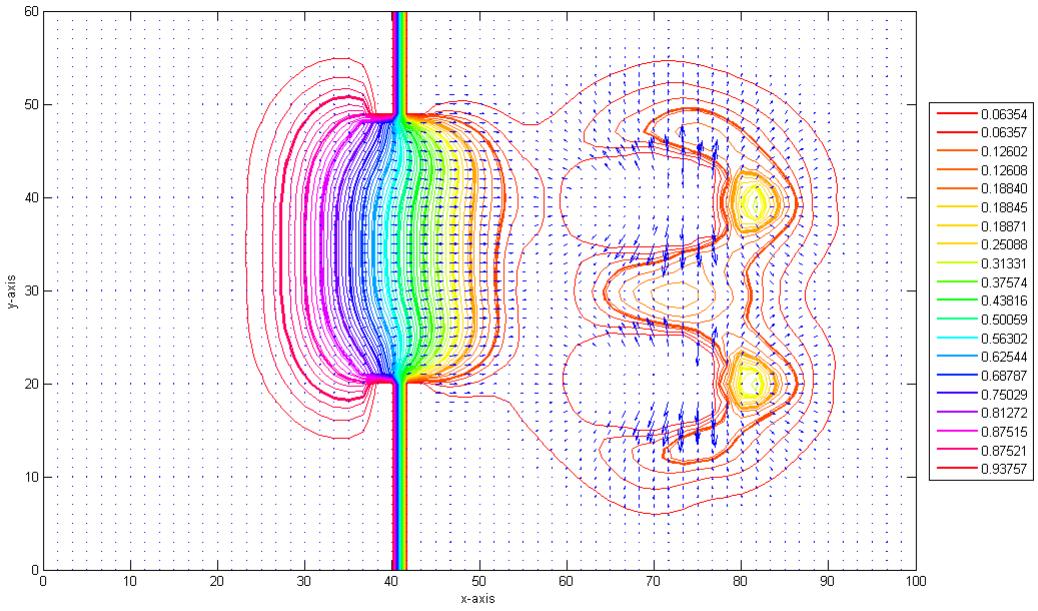

Figure 5.16: Water depth contours in a dam break scenario with entrainment.

The figure 5.18 shows the flood depths contours for a scenario of a dam break with the entrainment at the regions $x = 50$ to $x = 100$, while the figure 5.19 shows zoomed velocity vector plots and the flood depths distribution for scenario of the dam break without the entrainment in the same region.

The figure 5.20 shows the velocity vector plots of a dam break scenario without entrainment. The attached key shows the magnitudes of the non-dimensional values of the velocity at various locations on the topography. The velocity of water waves is relatively high at the exit of the breach, but low adjacent to the mounds (no-slip condition) as compared to the region away from the mounds. The velocity decreases as the water wave progresses downstream of the breach location. However it may be noted that the velocity

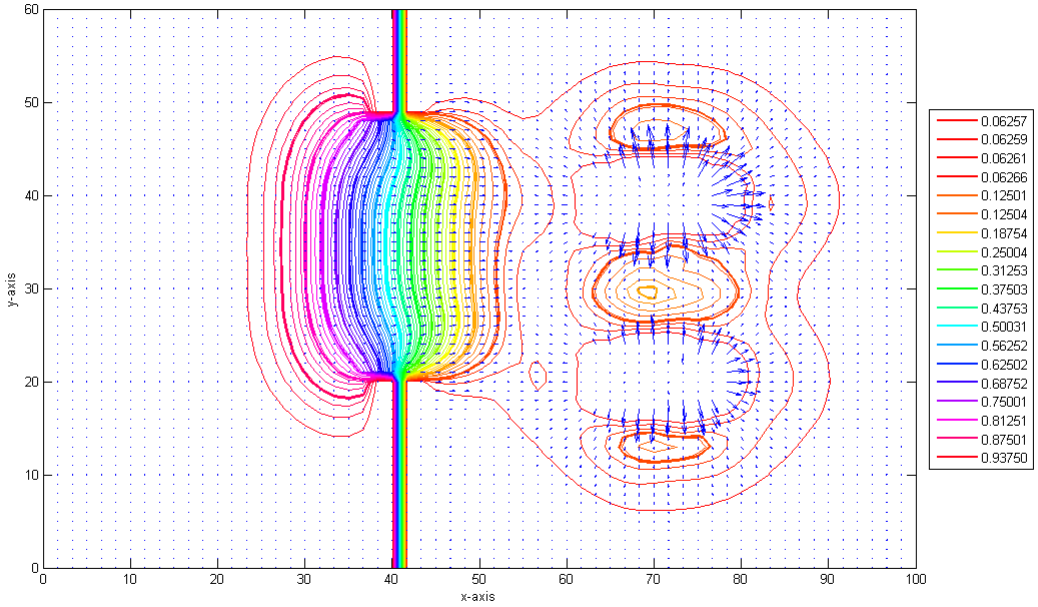

Figure 5.17: Water depth contours in a dam break scenario without entrainment.

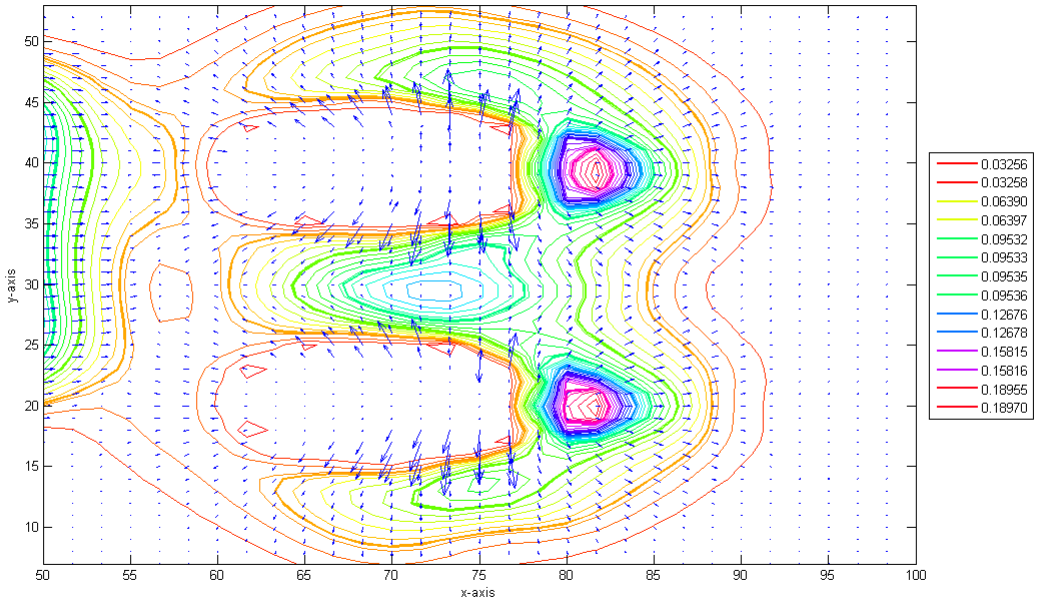

Figure 5.18: Zoomed water depth contours in a dam break scenario with entrainment.

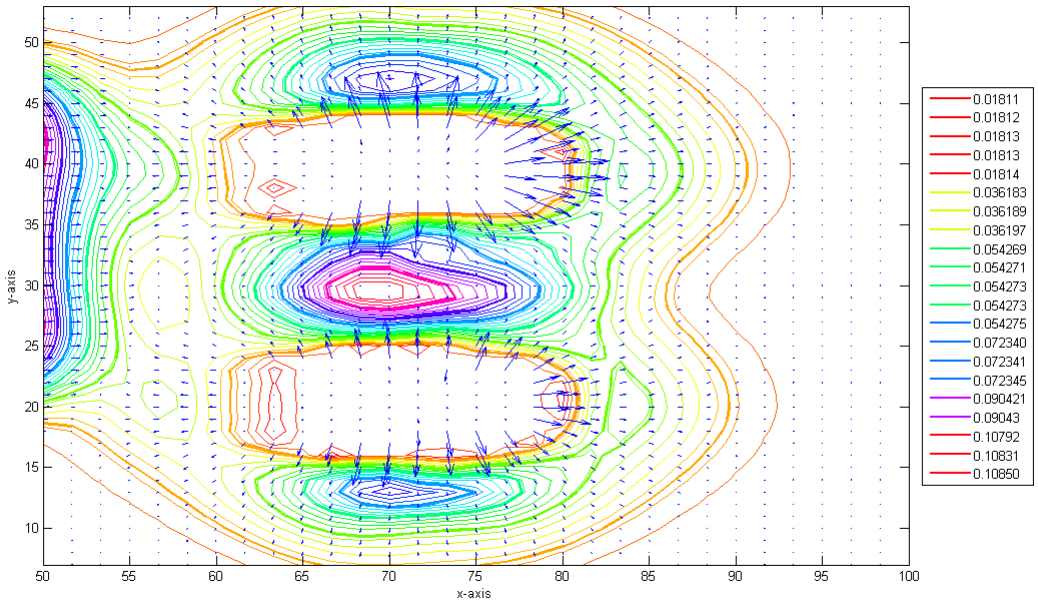

Figure 5.19: Zoomed water depth contours in a dam break scenario without entrainment.

magnitudes are comparatively lower for the case with entrainment than without the entrainment. This is because of the more massive bed load carried in the case of the dam break scenario with the entrainment.

The figure 5.21 is the aerial view of the mounds before and after the dam break scenario with the entrainment. Its clear that after the dam break the original mounds were eroded and changed the shape. The eroded sediments load was deposited near the mounds and within the vicinity of the mounds.

The figure 5.22 is the aerial view comparing the topographic surface of the mounds before and after dam break scenario without the entrainment.From the figure its observed that there is a morphological evolution of the mounds due to the shearing force and the scouring effects caused by the flow. Comparing the figures 5.21 and 5.22 it is clear that the morphological change of the

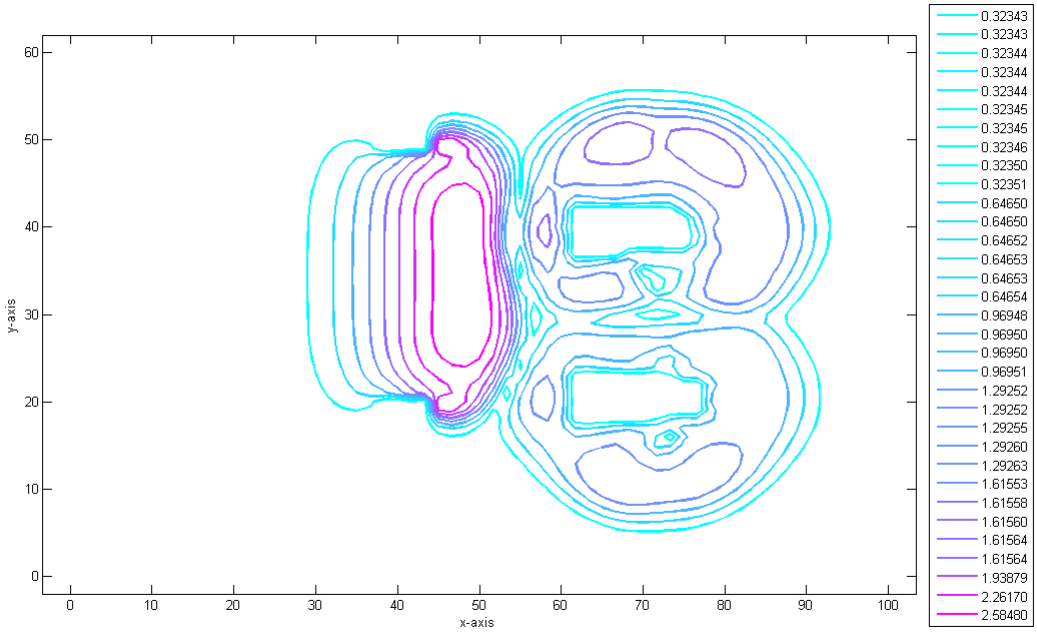

Figure 5.20: The Velocity vector plots and the magnitudes of the velocity.

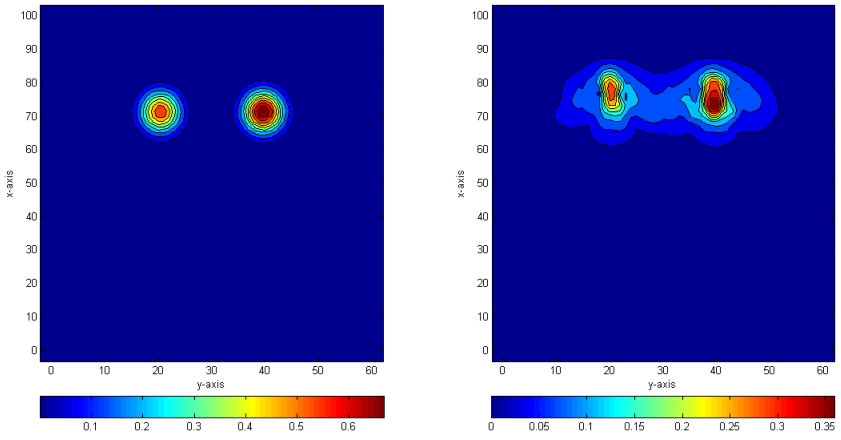

Figure 5.21: Aerial view of the topography before dam break (left) and after dam break (right) scenario with the entrainment.

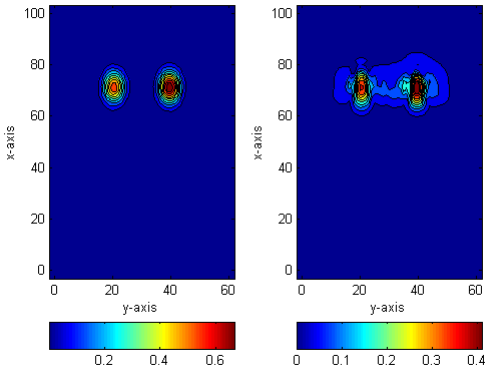

Figure 5.22: Aerial view of the topography before dam break (left) and after dam break scenario (right) without entrainment.

mounds is more in the case of the dam break scenario with entrainment than without the entrainment. This is because in the entrainment flow there is more scouring effects and thus higher bed load transport than for the flow without the entrainment.

The figure 5.23 shows the hydro graphs comparing the profiles of the morphological evolution of the mounds at three different scenarios. The blue hydro graph represents profile of the original mounds before the dam break, the black hydro graph represents the profile of the morphological evolution of the mounds in a dam break scenario without entrainment while the red hydro graph represents the profile of the morphological evolution of the mounds in a dam break scenario with the entrainment. It can be observed that the morphological evolution is more intense in the case of the dam break scenario with the entrainment than without the entrainment.

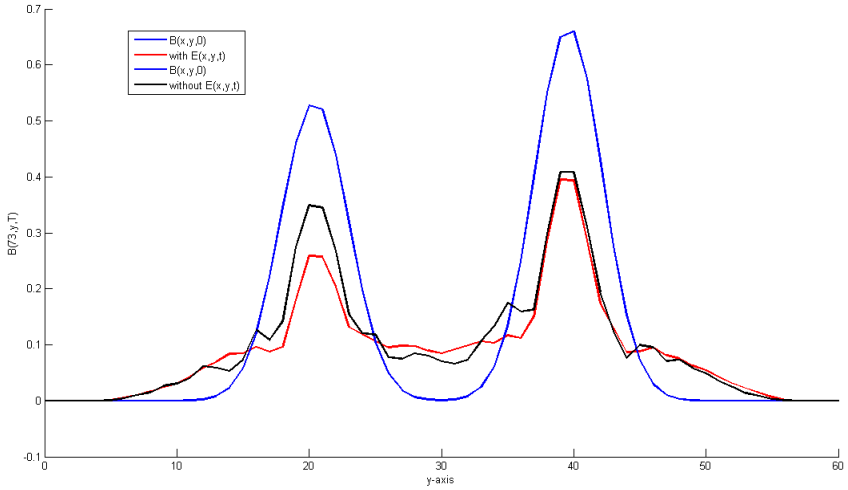

Figure 5.23: The profiles comparing the morphological evolution of the mounds.

5.3 Conclusion

A model capable of simulating dam break flows on a topography containing a narrow deep furrow with and without entrainment and dam break flows on a topography containing two mounds located on the downstream location of dam breach has been developed. The numerical model was developed by coupling shallow water equations with the bed-update equation and the entrainment equation. These equations were then non-dimensionalized and formed the governing equations which are a set of highly non-linear hyperbolic partial differential equations. To solve these equations a numerical model was developed using a relaxation scheme. The relaxation scheme involved three steps, first the set of non-linear hyperbolic equations were relaxed using the relaxation (artificial) variables, U, V, W, i.e. the non-linear hyperbolic equations were converted to linear hyperbolic equations. Secondly the relaxed equations were discretized spatially (semi-discretization), using the Vanleer's MUSCL scheme which is total variation diminishing (TVD) and thirdly the

time discretization, full discretization was performed using the implicit-explicit fourth order Runge kutta scheme.

From the results of the simulations we conclude that;

1. The flood inundation is higher for the dam break scenario with entrainment than in the dam break scenario without the entrainment. This is possibly due to the fact that for dam break scenario with the entrainment, velocity of the water waves was less than the threshold entrainment velocity u_c.

2. In both dam break scenarios, with the entrainment and without the entrainment, there was a physical change of the topography containing the furrow, i.e. the furrow had undergone morphological evolution. The furrow widened due to the shearing force of the water flow and became shallower due to the deposition of the bed load at the bottom. However comparing the two scenarios of the dam breaks, the morphological evolution of the furrow is more intense in the scenario of a dam break with entrainment than without the entrainment.

3. There was a higher deposition of the bed load at the furrow end in the case of the dam break scenario with the entrainment than in the dam break scenario without the entrainment. This could be explained using the law of conservation of mass (bed-update equation 3.74) i.e the bed load eroded through the scouring effects was conserved.

4. The flood depths was higher near the region with the obstacles and decreased further away downstream. This is possibly because the mounds

acted as the barrier of the water flow and hence the rise of the flood depths in those regions.

5. The down stream effects of flooding for a dam break scenario with the entrainment had more damaging effects on the mounds than in the dam break scenario without the entrainment.

6. Comparing the magnitudes of the velocities it is observed that the velocities are higher in the dam break scenario without entrainment than in the dam break scenario with the entrainment in both topographic surfaces.

7. The entrainment thus significantly affects the flow dynamics and morphological evolution

Therefore the model developed is quite conservative, robust, efficient, and has produced very good results which are in agreement with documented ones and consistent with the field observations. The present model can therefore be very useful to the government and to the non-governmental bodies such as Red Cross societies because they provide vital information on disaster management and emergency action plans such as;

1. The flood depth contours can be used to compile a flood inundation mapping which could help the communities in the areas prone to flood on how to protect lives and property by providing tools and information to help them understand their local flood risks and make cost-effective mitigation decisions.

2. The flood inundation maps can also be uploaded on the website and provide crucial information to the concerned bodies to visualize potential

flooding scenarios, identify areas and resources that may be at risk, and enhance their local response effort during a flooding event.

3. The information could be used by the hydraulic engineers to access the hydraulic structures damaged or blocked by floating objects, and also to identify critical infrastructures such as treatment plants, pumping stations, industrial complexes, electricity substations, telecommunications exchanges etc and vulnerable public buildings such as schools, hospitals etc. which are located in the flood risk areas.

4. Identifying the location of transit areas and temporary rest centres for evacuation purposes, areas of flood defence resources (equipment, sand bags etc) and the extent of and depth of flooding.

5. The magnitudes of the velocity in velocity vector plots can provide a vital information on the least time expected for the flood downstream to reach the mounds (infrastructures) in the down stream locations.

6. The damaging effects of the topography containing the furrow and mounds (morphological evolution of furrow and mounds) can provide vital information on the extent of damage which would occur with time on important historical sites such as harbours.

7. The flood depth contours can also provide important information to the structural engineers in determining the building's base flood elevation (BFE), i.e. the elevation at which the building has a chance of flooding annually.

8. Therefore the model developed could be used to formulate proper emergency action plans to minimize flood impacts within the economic life time of the assets.

5.4 Recommendations for further research

For future work we propose some improvements for the shallow water equations model possibly in the following two ways;

1. By using an unstructured grid to simulate the flows within the growing furrow and around the deforming mounds.

2. By introducing more physics in the sediment layer by considering a more complete system for which the concentration equation can be exhibited. This could be done by considering a formal reduction procedure starting from the three-dimensional model see Gerbeau and Benoit (2001) or by directly introducing adapted multi layer models see, Zech *et al.* (2008).

3. By improving a fluid model which is shear free and that which could admit instability (since SWEs are averaged models and do not admit instability) arising on the bed from initial perturbations.

References

Ahmad, M., M.Mamat, Nik, W. W., and Kartono, A. (2013). Numerical method for dam break problem by using godunov approach. *International Journal of Applied Mathematics and Computer 2: 95-107.*

Anderson, D., Tunnehill, J., and Pletcher, R. (1984). Computational fluid mechanic and heat transfer. *Hemisphere 59: 307-328.*

Audusse, E., Delestre, O., Mason, M., Navaro, P., and Serra, R. (2013). Parallelization of a relaxation scheme modelling the bedload transport of sediments in shallow water flow. *Journal on Computing Physics 408: 78-90.*

Biscarini, C., Francesco, S. D., and Manciola, P. (2010). Cfd modelling approach for dam break flow studies. *Hydrological Earth System of Sciences 14: 705-708.*

Brufao, P., Garcia, P., and Vazquez, C. (2004). Zero mass error using unsteady wetting-drying conditions in shallow water flows over dry irregular topography. *International Journal for Numerical Methods in Fluids 45: 1047-1082.*

Brufao, P. and Navarro, G. (2003). Unsteady free surface flows over complex topography with a multidimensional upwind technique. *Journal on Computing Physics 186: 503-526*

Brufao, P., Vazquez-Cendon, M., and P.Garcia-Navarro (2002). A numerical model for the flooding and drying of irregular domains. *International Journal for Numerical Methods in Fluids 39: 247-275.*

Chalabi, A. (1999). Convergence of relation schemes for hyperbolic conservation laws with stiff source terms. *Mathematics of Computation 68: 955-970.*

Delis, A. and Katsaounis, T. (2003). Computational methods for 2d shallow water flows based on relaxation schemes. *International Journal for Numerical Methods in Fluids 41: 695-719.*

Delis, A. and Katsaounis (2005). Numerical solution of the two-dimensional shallow water equations by the application of relaxation methods. *Science direct 29: 754-783.*

Diaz, M. C., Fernadez-Nieto, C., and Ferreiro, A. (2008). Sediment transport models in shallow water equations and numerical approach by high order finite volume methods. *Computer and Fluids 52: 620-635.*

Fennema, R. and Chaudhry, M. (1990). Explicit methods for 2-d transient surface flows. *Journal of Hydraulic Engineering 116: 1013-1034* .

Fread, D. (1993). *Flow Routing in Handbook of hydrology.* Number 10.1-10.36. Mcgrawhill., Newyork USA.

Gerbeau, J. and Benoit, P. (2001). Derivation of viscous saint-venant system for laminar shallow water; numerical validation. *Discrete Continuum and dynamical system. Series B.*

Grass, A. (1981). Sediment transport by waves and currents. *SERC London, Central Marine Technological Report No: FL29.*

Hudson, J. and Sweby, P. (2003). Formulations for numerically approximating hyperbolic systems governing sediment transport. *Journal on Computing Physics 19: 225-252.*

Hussain, S. and Rai, N. (2000). One dimensional dam break flood analysis for kameng hydro elctric project, india. *International Seminar and Workshop, session 2: Mathematical Modelling to simulate a dam break flood, Seinajoki, Finland.*

Jean-Marie, Z. and Azzeddine, S. (2010). Modelling of wetting-drying transitions in free surface flows over complex topographies. *Computer Methods in Applied Mechanics and Engineering 44: 301-319.*

Jin, S. and Levermore, C. (1996). Numerical schemes for hyperbolic conservation laws with stiff relaxation terms. *Journal on Computing Physics 126: 449-467.*

Jin, S. and Xin, Z. (1995). The relaxation schemes of conservation laws in arbitrary space dimensions. *International Journal on Pure Applied Mathematics 48: 235-277.*

Lachouette, D., Bonelli, S., Golay, F., and Seppecher, P. (2009). Numerical modelling of interfacial soil erosion. *Imath laboratory, University of the South Toulon-Var, La Garde, France 73: 555-578.*

Mingham, C. and Causon, D. (June, 1998). High-resolution finite-volume method for shallow water flows. *Journal of Hydraulic Engineering 124: 605-614.*

Richardson, S., T.Pullen, and Clarke, S. (2002). Jet velocities of overtopping waves on slopping structures: Measurements and computation. *In preceedings of the 28th International conference on Coastal Engineering.*

Simpson, G. and Castelltort, S. (2006). Coupled model of surface water flow, sediment transport and morphological evolution. *Computers and Geosciences 32: 1600-1614.*

Singh, J., Altinakar, M. S., and Ding, Y. (2011). Two-dimensional numerical modelling of dam-break flows over natural terrain using a central explicit scheme. *National Centre for Computational Hydroscience and Engineering 34: 1366-1375.*

Singh, V. (2005). Two-dimensional sediment transport model using parallel computer. *National Centre for Computational Hydroscience and Engineering 23: 1049-1077.*

Spiegiel, M. and Liu, J. (1999). *Mathematical Handbook of formulas and Tables.* Mcgraw-Hill ISBN 0-07-038203-4.

Zech, Y., Soarez-Frazao, S., Spine, B., and Le Grelle, N. (2008). Dam-break induced sediment movement: Experimental approaches and numerical modelling. *Journal of Hydraulic Research* 76: 193-222.

Zhou, J., Causon, D., Mingham, C., and Ingram, D. (2004). Numerical prediction of dam-break flows in general geometries with complex bed topographies. *Journal of hydraulic engineering 168: 1-25.*

Zoppou, C. and Stephen, R. (1991). Catastrophic collapse of water supply reservoirs in urban areas. *Mathematics Subject Classification 125: 686-695.*

Appendix A

Summary of Equations

A.1 Formula for solving the cubic functions

To solve the cubic function we consider the general cubic equation

$$P(x) = x^3 + a_1x^2 + a_2x + a_3 = 0 \tag{A.1}$$

Let

$$Q = \frac{1}{9}(3a_2 - a_1^2), R = \frac{1}{54}(9a_1a_2 - 27a_3 - 2a_1^3) \tag{A.2}$$

Then the discriminant is

$$\Delta = Q^3 + R^2 \tag{A.3}$$

and if

1. $\Delta > 0$ then one root is real and two are complex
2. $\Delta = 0$ then all roots are real and two are equal
3. $\Delta < 0$ then all roots are real and unequal

If the discriminant, $\delta < 0$ then the roots of $P(\lambda)$ can be determined by using

$$x_1 = 2\sqrt{(-Qcos\frac{1}{3}\theta)} - \frac{1}{3}a_1 \tag{A.4}$$

$$x_2 = 2\sqrt{(-Qcos\frac{1}{3}\theta)} + 2\phi) - \frac{1}{3}a_1 \tag{A.5}$$

$$x_3 = 2\sqrt{(-Qcos\frac{1}{3}\theta)} + 4\phi - \frac{1}{3}a_1 \tag{A.6}$$

where

$cos\theta = \frac{R}{\sqrt{-Q^3}}$